Renewable and Sustainable Energy Reviews 191 (2024) 114160

Contents lists available at ScienceDirect

Renewable and Sustainable Energy Reviews

journal homepage: www.elsevier.com/locate/rser

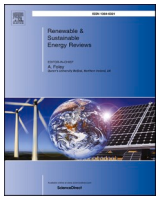

Dynamic reconfiguration of photovoltaic array for minimizing mismatch loss

Xiaolun Fang [a], Qiang Yang [b,*]

[a] School of Automation, Hangzhou Dianzi University, Hangzhou 310018, China
[b] College of Electrical Engineering, Zhejiang University, Hangzhou 310027, China

ARTICLE INFO

Keywords:
Photovoltaic array reconfiguration
mismatch conditions
Multiple switching matrices

ABSTRACT

Mismatch conditions owing to different internal and external factors, such as partial shading and module defects, can directly degrade the power generation of distributed photovoltaic arrays. In this study, a reconfiguration solution called multiple switching matrices is proposed to mitigate mismatch losses for any size of the total-cross-tied photovoltaic array. In the proposed solution, the photovoltaic array is divided into several sub-arrays using switching matrices. The current and voltage values of each module are collected by the electric measurement sensors and sent to the control unit, and the proposed reconfiguration solution can be implemented by controlling switching matrices. The performance of the proposed reconfiguration solution is evaluated extensively for a range of mismatched conditions, including partial shading patterns and partial shading with random failure patterns. The P–V and I–V characteristics are analyzed by comparison with the existing sudoku-based arrangement and the conventional total-cross-tied interconnection topology. Moreover, three main parameters and standard deviations of the maximum power point for each pattern, are considered. The numerical results confirm the effectiveness and flexibility of the proposed reconfiguration solution for optimizing photovoltaic array generation under various mismatch conditions.

1. Introduction

Owing to the exhaustion of fossil fuels and the worldwide pursuit of low-carbon energy provision, tremendous amounts of distributed renewable energy generation sources have been installed and used in the past decade [1]. Statistics from China's National Energy Administration indicate that the distributed solar generation infrastructure in China has increased by 29 GW and reached an installed capacity of 107.5 GW in 2021 [2]. Distributed photovoltaic (PV)-based solar power generation is playing an increasingly important role in environmentally friendly energy provisions. However, technical challenges exist in the operation of distributed PV systems [3], and one of the most urgent issues that must be addressed is array mismatch losses. PV arrays are composed of many PV modules, and mismatch losses in PV arrays may occur when the I–V characteristics of individual modules are significantly different. This is because the current is limited by the current of the lowest-current module when the PV modules are connected in series. Mismatch losses can directly lead to power generation degradation in the PV array and introduce multiple peaks in P–V characteristics with additional complexities to implement maximum power point tracking [4]. In practice, mismatch losses are frequently caused by shading or module defects. Previous studies [5] indicated that mismatch losses caused by moving clouds do not lead to serious power generation degradation for large-scale PV plants. However, mismatch losses, such as partial shading due to trees, buildings, and poles, always occur in distributed PV generation systems installed in complex environments. In addition, compared with large-scale PV plants, distributed PV systems lack regular cleaning, inspection operation, and maintenance, and mismatch loss problems, such as manufacturing tolerance, module defects, and dust on PV modules, are often observed in practice [6].

Monitoring PV systems is essential for reliable operation and maximum power generation, and collected measurements can be used for PV performance assessment and troubleshooting [7]. In this study, the voltage and current of the PV modules were measured in real-time using the deployed field sensors. This awareness of PV system generation can be used in the proposed dynamic topology optimization for power generation maximization under mismatched loss conditions.

PV-array reconfiguration technique is an attractive technique, which can effectively handle the mismatch loss problem for different topologies such as total-cross-tied (TCT) and series–parallel (SP) under mismatch conditions (MCs) [8]. The reconfiguration strategy can

* Corresponding author.
E-mail address: qyang@zju.edu.cn (Q. Yang).

https://doi.org/10.1016/j.rser.2023.114160
Received 10 November 2022; Received in revised form 2 December 2023; Accepted 6 December 2023

Nomenclature

i	The row numbers
j	The column numbers
k	The switching matrix numbers
G_0	Standard irradiance
G_{ij}	Irradiance received by module ij
I_{m}	Current generated by the module at the standard irradiance
I_{rowi}	Current output limit of the ith row
V_a	PV array voltage
$V_{\mathrm{m},i}$	Maximum array voltage at ith row
I_{ij}	Current values of the module ij
V_{ij}	Voltage values of the module ij
$\alpha/\ I_0/\ \eta V_T$	Parameters for irradiance estimation
$\mathbf{G}$	Irradiance matrix
$\mathbf{G}_k$	Irradiance sub-matrices
$\mathbf{G}_{\mathrm{R}}$	Row irradiances of irradiance sub-matrices
$\mathbf{I}_y$	Permutation matrices
$I_{y.ij}$	Elements in the permutation matrices
$\mathbf{G}_{\mathbf{new}}$	New irradiance matrix
G_i	The ith row irradiance
G_{ave}	The average row irradiance
f_r	The rth objective function
λ	Index weights of the objective functions

Abbreviation

PV	Photovoltaic
MCs	Mismatch conditions
TCT	Total cross-tied
SP	Series–parallel
EAR	Electrical array reconfiguration
MSM	Multiple switching matrices
MPP	Maximum power point
ML	Mismatch losses
ER	Execution ratio

change the interconnection between PV modules based on irradiance levels, and this flexibility in interconnection enables better mitigation of mismatch losses and enhances the overall performance of the PV system. The TCT and SP topologies are shown in Fig. 1(a) and (b), respectively. In the TCT topology, PV modules are connected in parallel in a row, and each row is connected in series. In the SP interconnection scheme, the PV modules are connected in series in a string and the PV strings are connected in parallel. Krishna [9] reviewed state-of-the-art PV-array reconfiguration strategies that fall into two main classes: physical relocation and electrical array reconfiguration (EAR).

The physical relocation technique involves relocating PV modules without altering any electrical connections. This process only requires a reconfigurable pattern for arranging the modules during installation, which helps distribute shading effects more effectively across the PV array. Solutions for physical relocation reconfiguration exist, the most notable of which is the sudoku puzzle. In Refs. [10,11], the sudoku puzzle method and an improved sudoku technique were used to relocate modules in a 9 × 9 TC T-interconnected PV array to improve power generation under partial shading conditions. However, the sudoku-based reconfiguration method can only relocate PV modules to a new position in a column but cannot change the position in a row. The futoshiki puzzle [12] and magic square [13] methods have the same limitations. Unlike previous solutions, a dominance square-based array reconfiguration scheme was proposed in Ref. [14] for a 5 × 5 TC T topology. The competence square arrangement method was proposed in Ref. [15] and was confirmed to perform better than the dominance square solution. In addition, a new PV array arrangement that uses numeric and alphabetic numbering was proposed in Ref. [16] to distribute shadow patterns over the entire PV array and minimize shading effects.

However, physical relocation-based reconfigurations have some limitations. The number of modules arranged in rows and columns must be equal in most physical configurations, for example, sudoku, competence square, and dominance square. In addition, another study [17] reported that non-uniform aging phenomena widely exist in PV modules and can degrade power generation in PV plants. This indicates that the effect of one-time physical reconfiguration will deteriorate as the module ages; hence, the physical relocation-based reconfiguration must be performed periodically (e.g., a couple of years), which demands tremendous human labor. Finally, such a reconfiguration solution is not sufficiently flexible to address the impact of multiple partial shadows and random module defects on the PV array power generation.

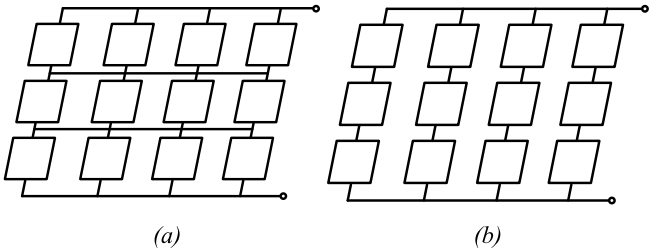

Fig. 1. PV array interconnection schemes: (a) TCT and (b) SP topologies.

In the case of the EAR, the environmental or electric parameters must20 be collected and analyzed, and the electrical connection of the PV array can be changed by controlling the switches. EAR can be implemented in two ways: global and local reconfiguration strategies. In the case of global PV array reconfiguration strategies, particle swarm optimization and genetic algorithm techniques were adopted to reconfigure a 9 × 9 TC T-based PV array to maximize power output in Refs. [18,19], respectively. In this method, each module can change its electrical connections to connect to any module in an adjacent column. An adaptive utility-interactive PV system based on a flexible switch matrix was developed in Ref. [20] to change the electrical connections between PV modules and DC/DC converters for a 3 × 3 PV array with an SP topology. However, the implementation of the reconfiguration methods in Refs. [18–20] requires more switches as well as sophisticated control algorithms that significantly increase the investment and maintenance costs. The amount of switches required increases with the expansion of the PV array, which can pose challenges for implementing a large-scale distributed PV system. Additionally, a switching matrix connecting the adaptive modules that can have an altered electrical connection with the fixed modules is used in the local reconfiguration process [21]. Similarly, using this structure, a fuzzy-partitioning-based intelligent reconfiguration approach was developed [22] to determine the optimal topology interconnection. Such a technique can reduce the number of switches; however, it cannot perform well under all shading conditions, for example, large shadowed areas or shadows that only appear on fixed modules.

In summary, the physical relocation technique does not require devices such as sensors and switches but only involves physically relocating during installation. However, due to the non-uniform aging of the PV modules, it is necessary to perform the physical relocation once again to ensure its effectiveness, which requires a significant amount of manpower. Additionally, the physical relocation technique can improve the power generation in conditions of concentrated shading, but it cannot guarantee efficiency under the MCs due to multiple shadows,

non-uniform aging and module failures. Therefore, it is necessary to study the EAR technique to avoid the use of a large number of switches, while improving the power generation efficiency for most MCs.

Thus far, this study proposes a multiple switching matrices (MSM) dynamic reconfiguration solution by controlling field-switching matrices to address the mismatch loss problem. In the proposed solution, the current and voltage values of each module are collected by the electric measurement sensors and sent to the control unit, and the proposed solution can be implemented by controlling switching matrices. Moreover, the proposed MSM solution can reconfigure a PV array for any number of rows and columns, and the number of switches used in this MSM solution is less than that in the global reconfiguration strategy, thereby reducing investment and maintenance costs. The main technical contributions of this study are as follows.

(1) An EAR solution, MSM, was developed in conjunction with the reconfiguration algorithm to address the mismatch loss problem of TCT-based PV arrays. This solution enables flexible alteration of PV module arrangements in distributed PV systems through the use of switching matrices, thereby significantly enhancing power generation under different MCs.
(2) The hardware-switching matrix structure is designed. The size of a switching matrix is only determined by the number of PV rows, independent of the number of PV modules in each row. Thus, the proposed solution is available for any PV array size.
(3) The proposed MSM reconfiguration solution was assessed and validated through extensive experiments under a range of mismatch conditions, considering different forms of partial shading and random PV module failure scenarios. Additionally, a cost–benefit analysis of the proposed MSM solution is presented.

The remaining sections are organized as follows: Section 2 introduces the modeling of the PV module and the TCT configuration. Section 3 presents the implementation of the proposed MSM reconfiguration solution. The design of various mismatch scenarios is described in Section 4, and a performance evaluation of the solution is presented in Section 5. Finally, Section 6 concludes the work.

2. TCT configuration of a PV array

2.1. Modeling of the PV module

The PV array comprises a set of PV modules, and each module consists of many cells. Modeling techniques are available for single-, double-, and three-diode models. In this study, a single-diode model is considered, as shown in Fig. 2 [23], and its mathematical model is given as

$$I = I_{ph} - I_0\left[\exp\left(\frac{q(V+IR_s)}{k\eta T}\right)-1\right] - \frac{V+IR_s}{R_{sh}} \tag{1}$$

where R_s and R_{sh} represent the series and shunt resistances, respectively.

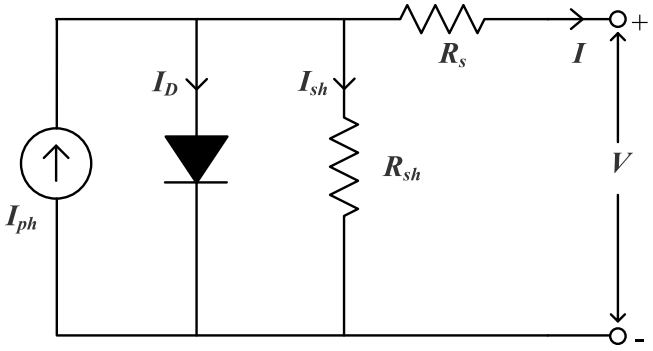

Fig. 2. Equivalent circuit model of a PV cell.

I and V represent the current and voltage generated by the PV cell, respectively; I_{ph} and I_0 represent the photocurrent and reverse saturation current, respectively; η is the diode ideality factor (typically between one and two for a single cell); k is the Boltzmann constant ($1.38\times10^{-23}J/K$); q is the elementary charge ($1.6\times10^{-19}C$); and T is the absolute temperature. Furthermore, the PV module was formed by connecting a number of PV cells in series and in parallel. The mathematical modeling of a PV module with N_p cells in parallel and N_s cells in series is given by as [14]

$$I = N_pI_{ph} - N_pI_0\left[\exp\left(\frac{q(V+IR_s)}{N_sk\eta T}\right)-1\right] - \frac{V+IR_s}{R_{sh}} \tag{2}$$

PV cells can be inorganic, organic, or organic–inorganic hybrid according to different materials. The photon-to-electron conversion efficiencies of PV cells differ for different materials. However, their external behaviors (P–V and I–V characteristics) are similar [24]. Moreover, the realization of the PV array reconfiguration strategies is based on the electrical parameters of each PV module. Therefore, the PV array reconfiguration strategy has the desired effect on both the organic and inorganic materials.

2.2. PV array with a TCT topology

For the PV array with a TCT topology, the PV modules in the same row are connected in parallel, and the PV modules in the same column are connected in series. The $n\times m$ TCT topology is shown in Fig. 3, where the labels indicate the locations of the modules. For example, '36' represents the module located in the third row and sixth column.

For the PV module 'ij,' the produced current can be calculated using

$$I_{ij} = k_{ij}I_{\mathrm{m}} = \frac{G_{ij}}{G_0}I_{\mathrm{m}} \tag{3}$$

where i and j correspond to the row and column numbers, respectively; G_{ij} represents the irradiance received by module ij. G_0 is the standard irradiance ($G_0 = 1000W/m^2$), and I_{m} is the current generated by the module at the standard irradiance. The maximum current of the row is equal to the sum of the current limits of each module because the PV modules in the same row are connected in parallel. Hence, the current output limit of each row is calculated using as

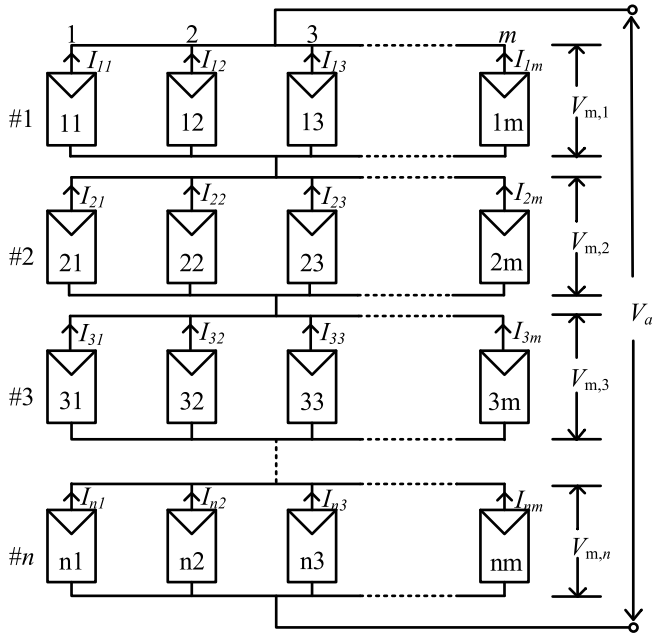

Fig. 3. TCT topology of a PV array.

$$I_{rowi} = \sum_{j=1}^{m} k_{ij} I_{\mathrm{m}} \tag{4}$$

where I_{rowi} represents the current output limit of the row $\#i$. According to Kirchhoff's Voltage Law, the array voltage of the TCT topology is the sum of the voltages in each row because the PV modules in the same column are connected in series. Hence, the array voltages for the nine rows were calculated using

$$V_a = \sum_{i=1}^{n} V_{\mathrm{m},i} \tag{5}$$

where V_a is the PV array voltage of the TCT topology, and $V_{\mathrm{m},i}$ represents the maximum array voltage at row $\#i$.

3. Proposed multiple switching metric-based optimal reconfiguration solution

To address the mismatch loss problem of a PV array with the TCT topology, this study proposes a novel reconfiguration solution, namely MSM. The basic idea behind this solution is as follows: The current and voltage values of each module are collected by electric measurement sensors and sent to the control unit. A TCT-based PV array can be organized into several parts connected by switching matrices that are controlled by a control unit with an optimization engine.

3.1. MSM reconfiguration solution

In the proposed MSM reconfiguration solution, the PV array is divided into k+1 parts through k switching matrices. The electricity connection within each part is fixed and each part is connected via a switching matrix. The proposed solution applied in a $n\times$ m PV array is shown in Fig. 4, and the positions of the electric measurement sensors (current and voltage) are illustrated in Fig. 5 (a) [25]. The design of the number of switching matrices is a tradeoff between cost and flexibility. This means that the more switching matrices, the better the effect of the PV array reconfiguration, but the higher the cost. Moreover, the positions of the switching matrices determine the number of PV columns in each part and affect the power generation after the PV array reconfiguration. Further, the design of the switching matrix is illustrated in Fig. 5 (b). For a PV array with n rows, the switching matrix consists of $n \times n$ sets of switches. When switch $S(i,j)$ is closed, the interface $L(i)$ is connected to interface $R(j)$. The size of a switching matrix is only determined by the number of the PV rows and is not related to the number of PV modules in each row. Thus, the proposed solution can be scaled and implemented for PV arrays of any size.

In the proposed solution, the negative effect of array mismatch on the PV array can be minimized using controllable switching matrices. As shown in Fig. 4, the system includes a control unit that controls the switching matrices. This control unit determines the optimal arrangement of the PV array using control and decision algorithms [8]. In the algorithmic solution, the voltage and current values of the PV modules are used as input variables, and the optimal module arrangement with the minimum difference in the row irradiance values is the output result.

In this study, MATLAB/Simulink was used to simulate the mismatch conditions and connection solution of the PV array with various solar irradiances. For the sake of limited space and clarity, a simulation model of a 3 × 4 PV array with a switching matrix as an example is presented in Fig. 6. From the figure, the voltage and current values of each model can be obtained using the measurement blocks. Input matrix ***ir*** represents the irradiance received by each PV model, and signal matrix ***sig*** controls the state of each set of switches. The control signal (i.e., the 'initial status' in the switch block parameter) '1' is defined as a closed contact and '0' is defined as an open contact.

A typical mismatch condition with two switch-control signals and the corresponding P–V and I–V characteristics are shown in Fig. 7. $S(1,1)$, $S(2,2)$, and $S(3,3)$ were closed before reconfiguration, and multiple peaks appeared in the P–V curve owing to the difference in the row irradiance values in the PV array. The states of the switches could be changed using control signals. After reconfiguration, $S(1,3)$, $S(2,2)$, and $S(3,1)$ were closed, the difference in the row irradiance values disappeared, and the PV curve had only one peak value.

3.2. Optimal reconfiguration algorithm

YALMIP is a MATLAB optimization toolbox that can be used to model and solve optimization problems that typically occur in control theory. It is easy to add solvers and new problem classes because of the flexible

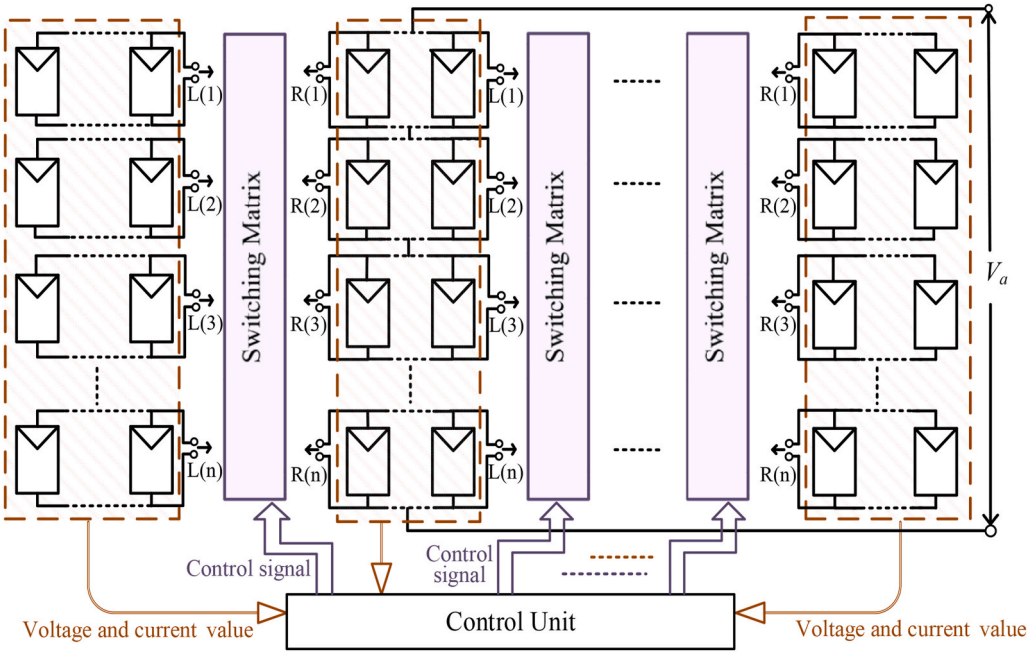

Fig. 4. Schematic illustration of the proposed MSM-based reconfiguration solution.

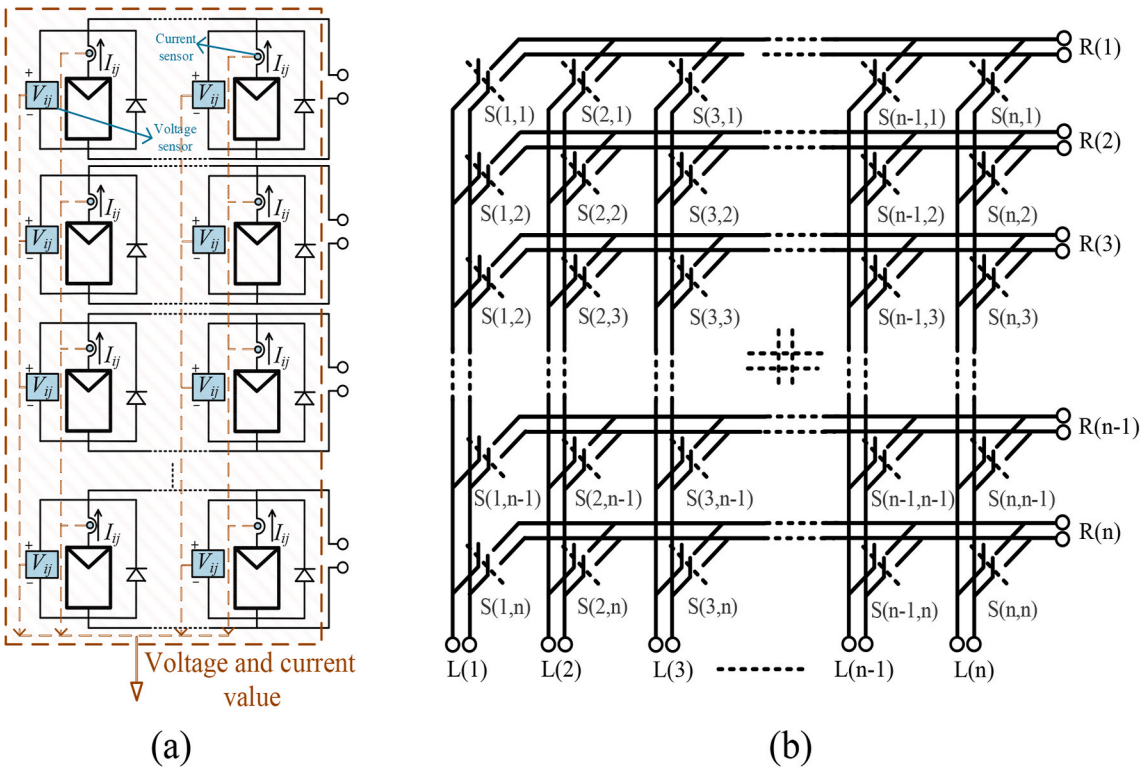

Fig. 5. Schematic diagram of sensor deployment and switching matrix design: (a) sensor positions in the PV array; and (b) structure of the designed switching matrix.

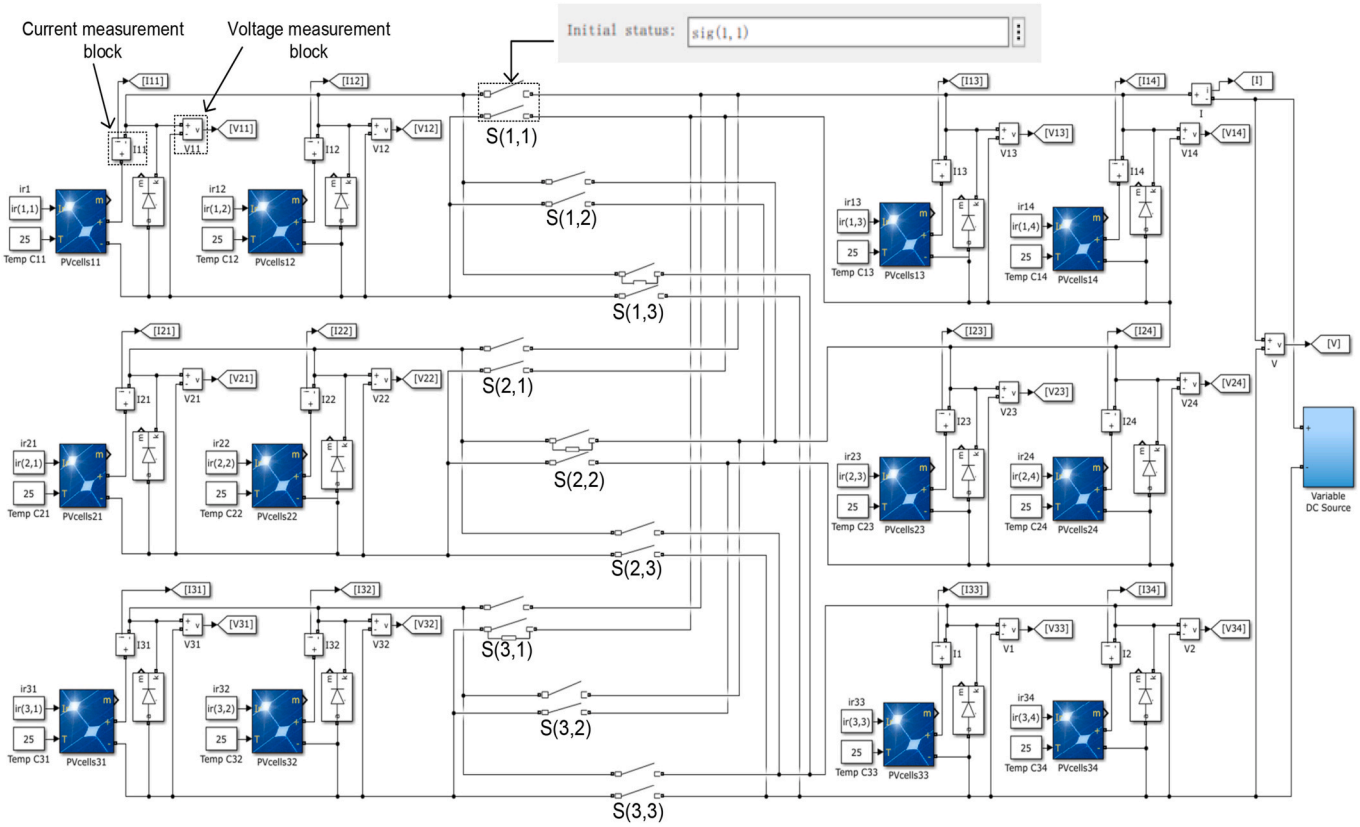

Fig. 6. Simulation model of a 3 × 4 PV array with a switching matrix.

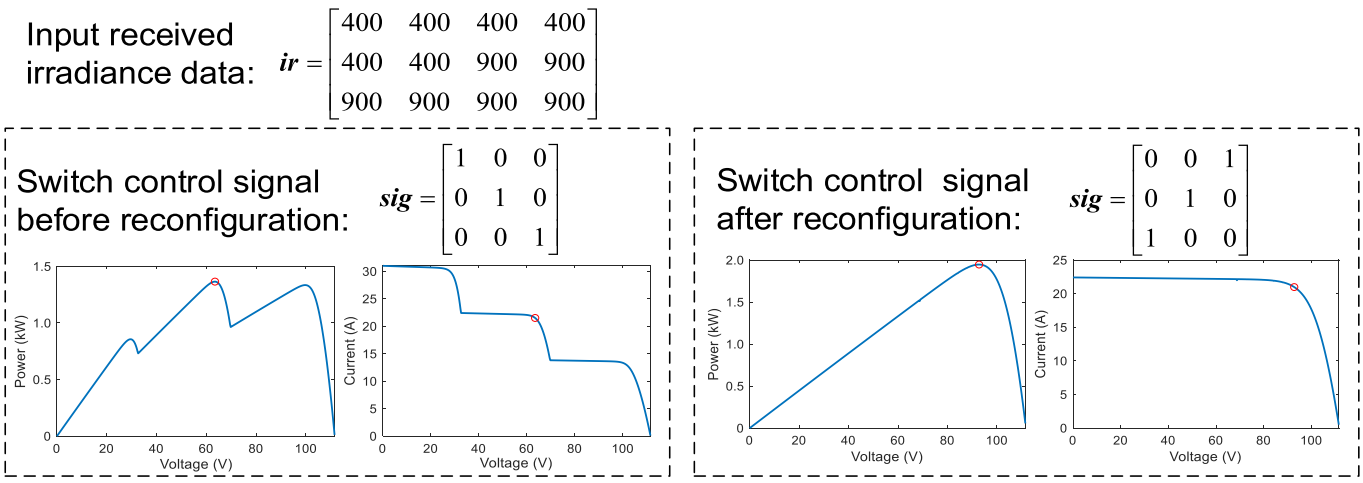

Fig. 7. P–V and I–V simulation curves for a typical mismatch condition with two switch-control signals.

solver interface and internal format [26]. Gurobi is a widely adopted solver dedicated to solving optimization or programming problems, including linear programming (LP), quadratic programming (QP), quadratically constrained programming (QCP), mixed-integer linear programming (MILP) and mixed-integer quadratically constrained programming (MIQCP) [27]. In this study, the proposed PV array reconfiguration solution was modeled in YALMIP and solved at the Gurobi interface.

Flowchart of the proposed MSM reconfiguration algorithm is illustrated in Fig. 8 and is described in detail as follows.

Step 1. Initialization

The $n \times m$ irradiance matrix '**G**' of the PV array and the number of switching matrices k are input.

Step 2. Irradiance estimation

The PV-array reconfiguration method relies on obtaining the irradiance information for each module through a separate sensor arrangement. Alternatively, the received irradiance values of individual modules can be estimated based on voltage and current measurements along with datasheet values [18], which can be expressed as

$$G_{ij} = \alpha\left[I_{ij} + I_0\left(e^{V_{ij}/\eta V_T} - 1\right)\right] y \tag{6}$$

where G_{ij} is the calculated irradiance received by the PV module ij, which is also the element of the i*th* row and jth column of matrix **G**. I_{ij} and V_{ij} denote the voltage and current values of the module ij, respectively. α, I_0, and ηV_T are the set of parameters that can be estimated from the manufacturer's datasheet values [28].

Step 3. Partition of the irradiance matrix

Based on the positions of the k switching matrices, the $n\times$ m irradiance matrix is divided into k+1 submatrices, which are represented by $\mathbf{G_1}, \mathbf{G}_2, \ldots, \mathbf{G}_{k+1}$.

Step 4. Definition of variables

Initialize the k+1 binary matrix variables of size $n \times$ n. These binary matrices are permutation matrices represented by $\mathbf{I}_1$, $\mathbf{I}_2$,… $\mathbf{I}_{k+1}$.

Step 5. Definition of constraints

The algorithm must constrain the binary matrix to a permutation matrix, that is, only one in each row and column and zero everywhere else.

$$\begin{cases} \sum_{i=1}^{n} I_{y,ij} = 1 \\ \sum_{j=1}^{n} I_{y,ij} = 1 \end{cases} \tag{7}$$

where $I_{y,ij}$ is the ith row and the jth column in matrix $\mathbf{I}_y$.

Step6. Obtainment of new solutions

The submatrix $\mathbf{G_1}, \mathbf{G}_2, \ldots, \mathbf{G}_{k+1}$ can change the position of the rows and obtain new submatrices, $\mathbf{G}_1^{'}$, $\mathbf{G}_2^{'}$, …,. $\mathbf{G}_{k+1}^{'}$ by multiplying the remaining permutation matrices, which can be expressed as

$$\mathbf{G}_y^{'} = \mathbf{I}_y \times \mathbf{G}_y, y = 1, 2, \cdots, k+1 \tag{8}$$

Then the new irradiance matrix is obtained by combining these k+1 new submatrices, denoted as '$\mathbf{G_{new}}$'.

Step 7. Calculation of row irradiance

The sum of each row element of the k+1 submatrix was calculated. The row irradiances of the k+1 irradiance sub-matrices are expressed as $\mathbf{G}_{R1}, \mathbf{G}_{R2}, \ldots, \mathbf{G}_{R(k+1)}$. Each element of the row irradiance matrix was calculated using Equation (9).

$$\begin{cases} G_{R1,i} = \sum_j G_{1,ij} \\ G_{R2,i} = \sum_j G_{2,ij} \\ \vdots \\ G_{R(k+1),i} = \sum_j G_{k+1,ij} \end{cases} \tag{9}$$

where $G_{R1,i}$, $G_{R2,i}$, …, $G_{R(k+1),i}$ is sum of the ith row elements of $\mathbf{G}_{R1}, \mathbf{G}_{R2}$, …, $\mathbf{G}_{R(k+1)}$, which represents the sum of the irradiance at the ith row of each part. $G_{1,ij}$, $G_{2,ij}$, …, $G_{k+1,ij}$ are the elements of ith and jth columns of $\mathbf{G_1}, \mathbf{G}_2, \ldots, \mathbf{G}_{k+1}$, respectively.

The sum of the irradiance at the i*th* row of the PV array is represented by G_i , which can be calculated as

$$G_i = G_{R1,i} + G_{R2,i} + \cdots + G_{R(k+1),i} \tag{10}$$

Step 8. Definition of the objective function

The performance of each interconnection scheme was evaluated based on the module irradiance. By using the variance of row irradiance as the objective function, the row irradiance of the PV array can be made relatively uniform, thereby reducing the mismatch loss, and the objec-

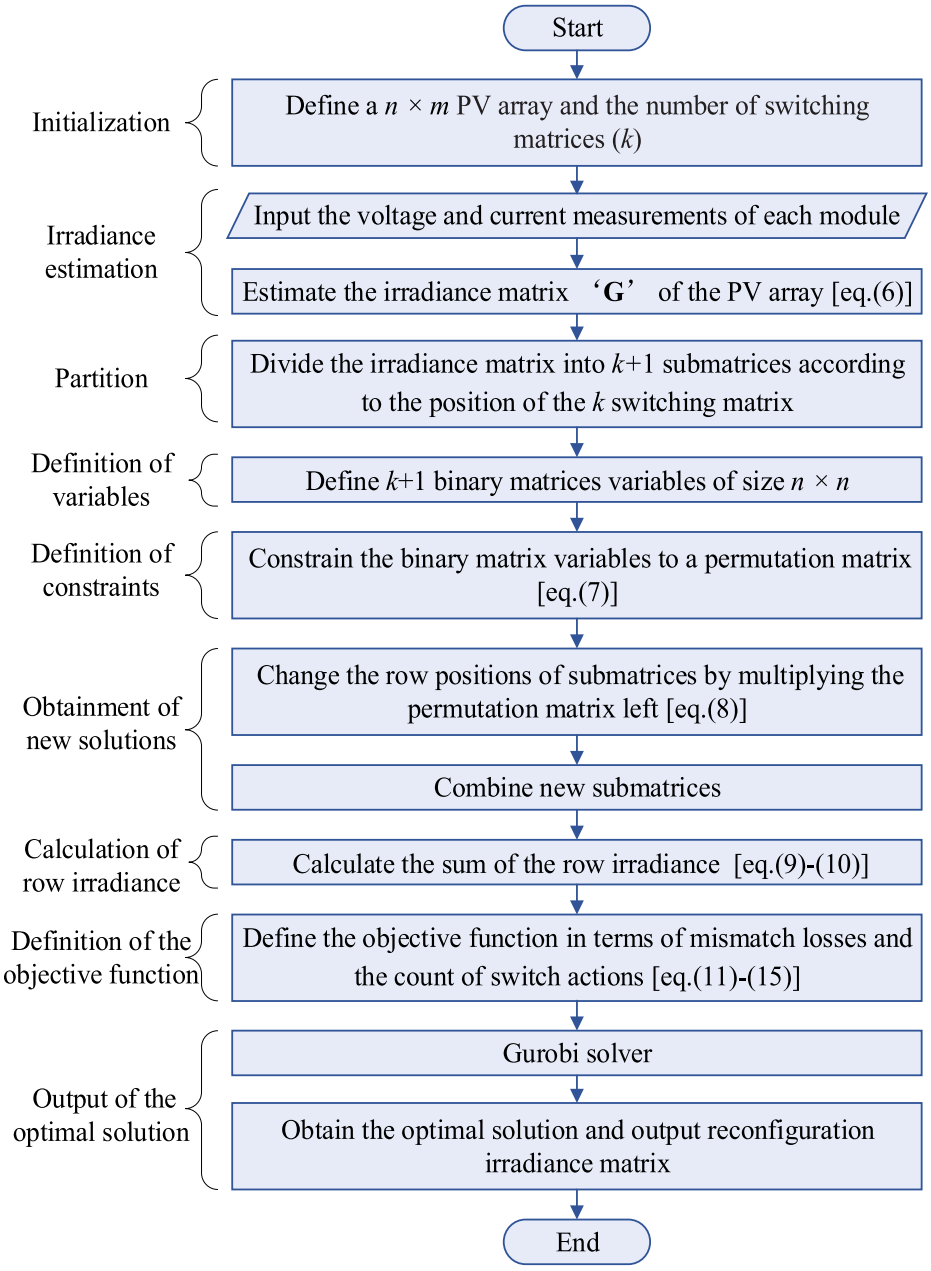

Fig. 8. Flowchart of the proposed MSM solution for the PV-array reconfiguration algorithm.

tive function can be expressed as

$$\min f_1 = \frac{1}{n}\sum_{i=1}^{n}(G_i - G_{\text{ave}})^2 \tag{11}$$

where G_{ave} is the average row irradiance, which can be represented by

$$G_{\text{ave}} = \frac{1}{n}\sum_{i=1}^{n} G_i \tag{12}$$

Another important indicator is the number of switch actions, and the objective function can be expressed as

$$\min f_2 = \sum_{y=2}^{k+1} \text{sum}\left(\text{abs}\left(\text{I}_y - \text{I}_{y-1}\right)\right) \tag{13}$$

where the function abs (·) is used to take the absolute value. The function sum (·) is used to sum the elements of a matrix.

Due to the inconsistent dimensions of the two objective functions, a reduced-half trapezoidal membership function is used in this study to normalize each objective function [29], and the expression of the minimum functions is shown in (14).

$$U(f_r) = \begin{cases} 0 & ,f_r \le f_r^{\min} \\ \dfrac{f_r - f_r^{\min}}{f_r^{\max} - f_r^{\min}}, f_r^{\min} & < f_r \le f_r^{\max} \\ 1 & ,f_r^{\max} < f_r \end{cases} \tag{14}$$

where $f_r^{\max}$ and $f_r^{\min}$ are the maximum and minimum values of the rth objective function, respectively, that is f_r. For f_1, the maximum value, $f_1^{\max}$, was the row irradiance variance of the initial PV-array irradiance matrix, and the minimum value, $f_1^{\min}$, was equals zero. For f_2, the maximum value, $f_2^{\max}$, is the count of times when all switches are in action, whereas the minimum value, $f_2^{\min}$, was equals zero. Then, the objective function of the PV reconfiguration algorithm can be expressed

as

$$\min OF = \lambda_1 U(f_1) + \lambda_2 U(f_2) \tag{15}$$

where λ_1 and λ_2 are the index weights of the objective functions f_1 and f_2, respectively. The optimization algorithm takes into account two factors. Objective function f_1 aims to improve the PV power generation, while objective function f_2 is designed to minimize the number of switch operations during each reconfiguration. The values of parameters λ_1 and λ_2 are determined by the algorithm requirement. In this study, improving the power generation of the PV array is considered the most significant factor, and $\{\lambda_1\ ,\ \lambda_2\} = \{1000, 1\}$ is used for the optimization process.

Step 9. Output of the optimal solution

The optimal solution with the minimum objective function value was identified using the Gurobi solver. Finally, the optimal solution for the reconfigured irradiance matrix was generated.

4. Mismatch pattern design

The proposed MSM reconfiguration solution was implemented and evaluated using simulation experiments. To evaluate the performance of the proposed solution, the specifications of the PV module used in this study are listed in Table 1, and a typical MSM scheme applied to a 9 × 9 PV array was tested. As shown in Fig. 9, this reconfiguration scheme contained two switching matrices, and the PV array was divided into three parts. From left to right, each part contained two, five, and two columns of the PV array, denoted as 'part A,' 'part B,' and 'part C,' respectively. In this reconfiguration scheme, the connections between the second and third columns and between the seventh and eighth columns were dynamic, whereas the rest were fixed electrical connections.

Furthermore, 32 different mismatch scenarios were considered to verify the effectiveness of the MSM reconfiguration solution. These 32 mismatch scenarios can be divided into two patterns: (1) partial shading pattern and (2) partial shading with a random failure pattern.

4.1. Partial shading pattern

In this study, sixteen different partial-shading scenarios, Cases I-1 to I-16, were considered, as shown in Fig. 10 (a). Four different irradiation levels, 900, 700, 400 and 200 W/m^2–were adopted in the performance evaluation. In these sixteen scenarios, the sum of the array irradiances was the same. Out of all the PV modules, ten modules were at 700 W/m^2, sixteen modules were at 400 W/m^2, six modules were at 200 W/m^2, and the remaining modules had an irradiance level of 900 W/m^2.

Here, Case I-1 represents a long and wide shadow where Rows 1–4 of the PV array is partially shaded. Case I-2 represents a long and narrow shadow, and Columns 7–9 of the PV arrays are partially shaded. Unlike the previous two cases, Cases I-3–I-6 represented two shadows of different sizes on the PV array. Cases I-7–I-12 represent six different scenarios with short and wide shadows at the two corners of the PV array. Cases I-13–I-16 represent the partial shading effect at the four corners of the PV array.

4.2. Partial shading with random failure patterns

Similarly, sixteen different partial shading cases with random failure patterns, that is, Cases II-1–II-16, were considered in this study, as illustrated in Fig. 10 (b). Based on the partial shading pattern, it was assumed that random failures occurred in three or four PV modules, with no power generation in the PV array. Similar to the previous pattern, the sum of the array irradiances was the same in these sixteen scenarios.

Table 1
PV module specifications.

Parameter	Value
PV power rating	249.85 W
Open circuit voltage	37.92 V
Short circuit current	8.62 A
Voltage at the MPP	30.96 V
Current at the MPP	8.07 A

5. Performance evaluation and numerical results

To evaluate the performance of the proposed MSM solution, the P–V and I–V curves were considered for the reconfiguration schemes. In this study, a 3.20 GHz AMD Ryzen 7 6800 H S CPU and 16.00 G RAM were used for the computational hardware, and the simulations were performed using MATLAB/Simulink (version 2018a). MIPGap, which represents the allowable gap, was set to 0.01 for the Gurobi solver. The decision-making time of the MSM solution for all tested scenarios was less than 5 s.

For each mismatch condition, the proposed reconfiguration solution was compared with the sudoku-based physical relocation reconfiguration and original TCT interconnection scheme. sudoku is a logic-based number puzzle consisting of a 9 × 9 square grid divided into nine 3 × 3 blocks (containing eighty-one cells). The goal of the sudoku puzzle is to fill in a 9 × 9 grid using nine digits such that each row, column, and each 3 × 3 block contains each digit only once. In the sudoku method, each module in the PV array can be represented by a number with two digits, where the first digit in the box represents the logic number and the second digit refers to the column number [11]; the pattern arrangement with the sudoku method is shown in Fig. 11.

In this study, owing to space limitations, four test cases (I-3, I-15, II-3, and II-15) were selected for the analysis. Three main performance metrics, the maximum power point (MPP), mismatch losses (ML), and execution ratio (ER), were adopted for the performance assessment of all test cases of the MCs. Furthermore, to compare the effects of different schemes, the standard deviations of the MPP of sixteen cases were calculated in the partial shading pattern and partial shading with a random failure pattern.

Mismatch losses are the difference between the sum of the maximum power output of each module and that of the PV array under MCs. The mismatch losses can be determined using (16)

$$ML = \sum_{i=1}^{n}\sum_{j=1}^{m} P_{ij} - GMPP_{MCs} \tag{16}$$

where $\sum_{i=1}^{n}\sum_{j=1}^{m} P_{ij}$ represents the sum of the maximum power output of each module.

The ER of a PV array is defined as the ratio of the MPP at the MCs to the MPP under standard test conditions (1000W/m^2, and 25°C), and can be calculated using

$$ER\ (\%) = \frac{MPP_{\mathrm{MCs}}}{MPP_{\mathrm{STC}}} \times 100\% \tag{17}$$

In statistics, standard deviation σ is used to quantify the dispersion of a dataset relative to its mean, and is calculated as the square root of the variance, which is expressed as

$$\sigma = \sqrt{\frac{1}{N}\sum_{i=1}^{N}(P_i - \overline{P})^2} \tag{18}$$

where N represents the number of variables, P_i represents the power output of Case i, and $\overline{P}$ represents the mean power output for all cases.

5.1. Partial shading patterns

1) Test case 1: two partial shadows (Case I-3)

The shadow position of the Case I-3 mismatch pattern in a 9 × 9 PV

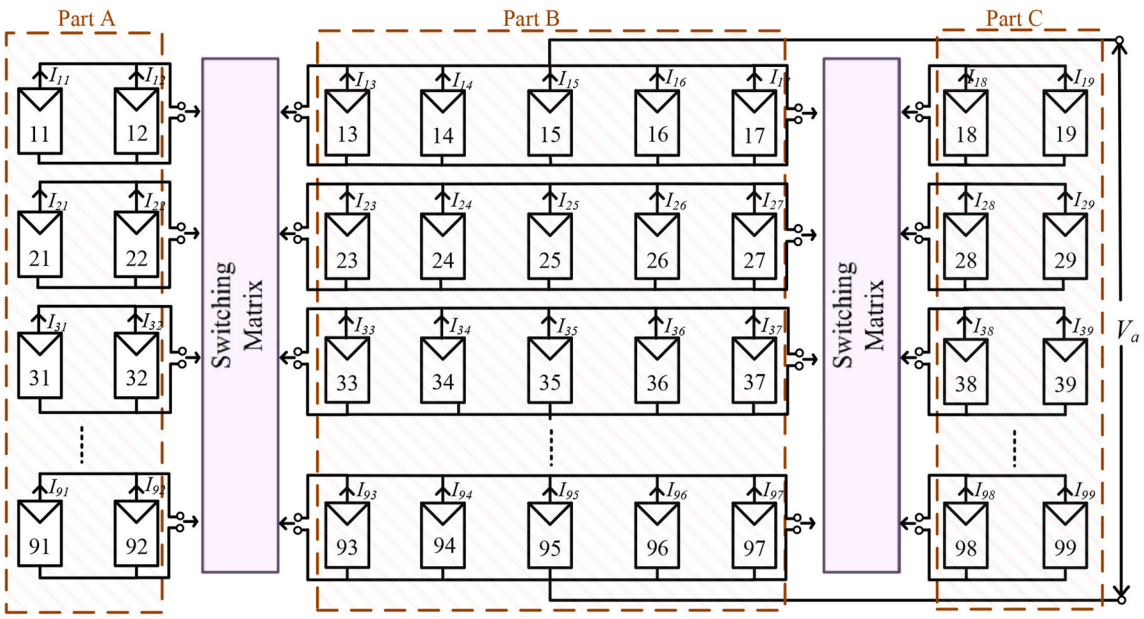

Fig. 9. Typical MSM reconfiguration scheme applied in a 9 × 9 PV array.

array is shown in Fig. 12(a). The arrangement realized using the sudoku-based physical reconfiguration is shown in Fig. 12(b). The arrangement after reconfiguration using the proposed MSM solution is shown in Fig. 12(c), where the number of switch actions was 24. Both the sudoku-based and MSM schemes distribute shaded modules within the array. This pheromone can effectively enhance the overall power generation of the PV systems.

Based on (3) and (4), the theoretical current in each row can be calculated according to the irradiance received by the PV module. Taking the TCT interconnection scheme of Case I-3 as an example, the currents of different rows can be calculated using (19)–(24).

$$I_{row1} = I_{row7} = 9\times\frac{900}{1000}I_m = 8.1I_m \tag{19}$$

$$I_{row2} = I_{row5} = 4\times\frac{900}{1000}I_m + \frac{700}{1000}I_m + 4\times\frac{400}{1000}I_m = 5.9I_m \tag{20}$$

$$I_{row3} = I_{row4} = 4\times\frac{900}{1000}I_m + \frac{700}{1000}I_m + 2\times\frac{400}{1000}I_m + 2\times\frac{200}{1000}I_m = 5.5I_m \tag{21}$$

$$I_{row6} = 4\times\frac{900}{1000}I_m + 3\times\frac{700}{1000}I_m + 2\times\frac{400}{1000}I_m = 6.5I_m \tag{22}$$

$$I_{row8} = 6\times\frac{900}{1000}I_m + \frac{700}{1000}I_m + 2\times\frac{400}{1000}I_m = 6.9I_m \tag{23}$$

$$I_{row9} = 5\times\frac{900}{1000}I_m + 2\times\frac{700}{1000}I_m + 2\times\frac{200}{1000}I_m = 6.3I_m \tag{24}$$

As the current in each row is different, there are multiple peaks in the P–V curve. Assuming that the MPP is located in the third row, that is, none of the modules are bypassed, the voltage of the array is $V_a = 9V_m$, and the power generation of the PV array is expressed as

$$P_a = I_{rowi}V_a = 5.5I_m \times 9V_m = 49.5V_mI_m \tag{25}$$

Assuming that the MPP is located in the second row, that is, two rows are bypassed, the voltage of the array is $V_a = 7V_m$, and the power produced by the array is expressed as

$$P_a = I_{rowi}V_a = 5.9I_m \times 7V_m = 41.3V_mI_m \tag{26}$$

The calculation of the MPP for each row is similar to Equations (25) and (26). To determine the location of the MPP for the three considered schemes, the details of the row current and corresponding power of the simulated PV array are presented in Table 2. The numerical results show that the power generation at the MPP was 49.5 V_mI_m, 49.5 V_mI_m and 54.0 V_mI_m in TCT, sudoku, and MSM schemes, respectively. Thus, the proposed reconfiguration solution can enhance the PV power generation through theoretical calculations in Case I-3.

The P–V and I–V characteristics of Case I-3 are shown in Fig. 13, where The MPP obtained for the proposed MSM reconfiguration solution is 14.250 kW, which is significantly improved, compared to the TCT interconnection scheme (13.380 kW) and the sudoku-based arrangement (13.539 kW). The proposed reconfiguration solution maintains a graceful I–V curve under mismatched conditions compared with the other two methods.

2) Test case 2: a corner shadow (Case I-15)

The shadow position of the mismatch scenario of Case I-15 is shown in Fig. 14(a). The arrangements realized by the sudoku method and proposed MSM solution are illustrated in Fig. 14(b) and (c), respectively. The number of switch actions in the proposed reconfiguration solution for this case was 20.

For these three schemes, the calculated voltage and current values and the obtained MPPs of the PV array are presented in Table 3. The MPP in the TCT interconnection scheme can be extracted when Rows 8 and 9 are bypassed, and the MPP in the sudoku-based arrangement and proposed reconfiguration solution can be extracted without bypassing. The numerical result shows that the TCT and sudoku schemes produce maximum power of 39.9 V_mI_m and 48.6 V_mI_m, respectively. The proposed reconfiguration solution generated a maximum power of 51.3 V_mI_m.

The P–V and I–V characteristics of Case I-15 are shown in Fig. 15. From the figures, the MPP obtained for the proposed MSM reconfiguration solution is 13.947 kW, which is an improvement over the TCT interconnection scheme (10.860 kW) and sudoku-based arrangement (13.419 kW). In addition, the I–V curve obtained using the MSM solution was more graceful than those obtained using the other two methods.

3) Statistics of all test cases (Cases I-1 to I-16)

Based on (16), (17), the MPP, ML, and ER values of the various schemes for Cases I-1 to I-16 are shown in Fig. 16 (a), (b), and (c),

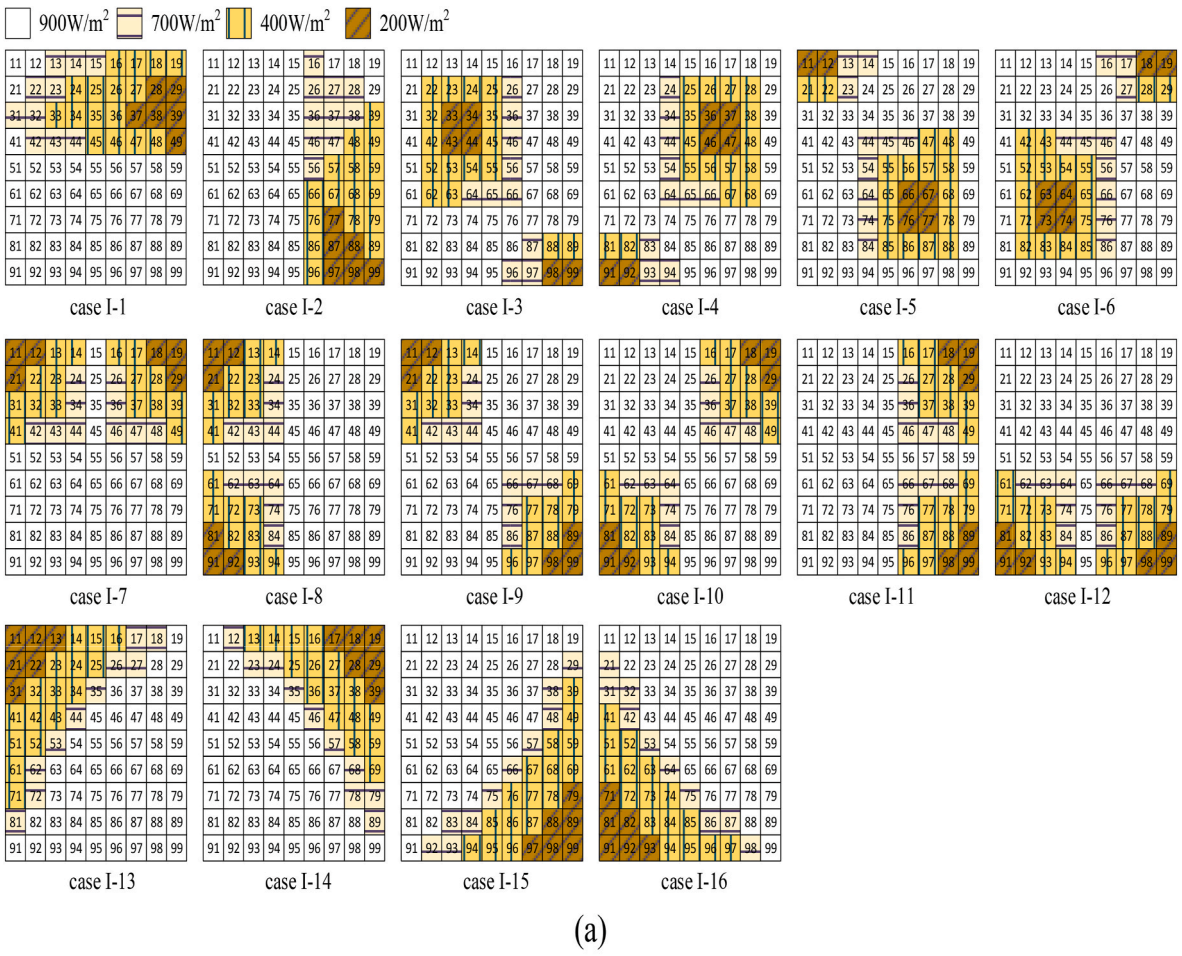

(a)

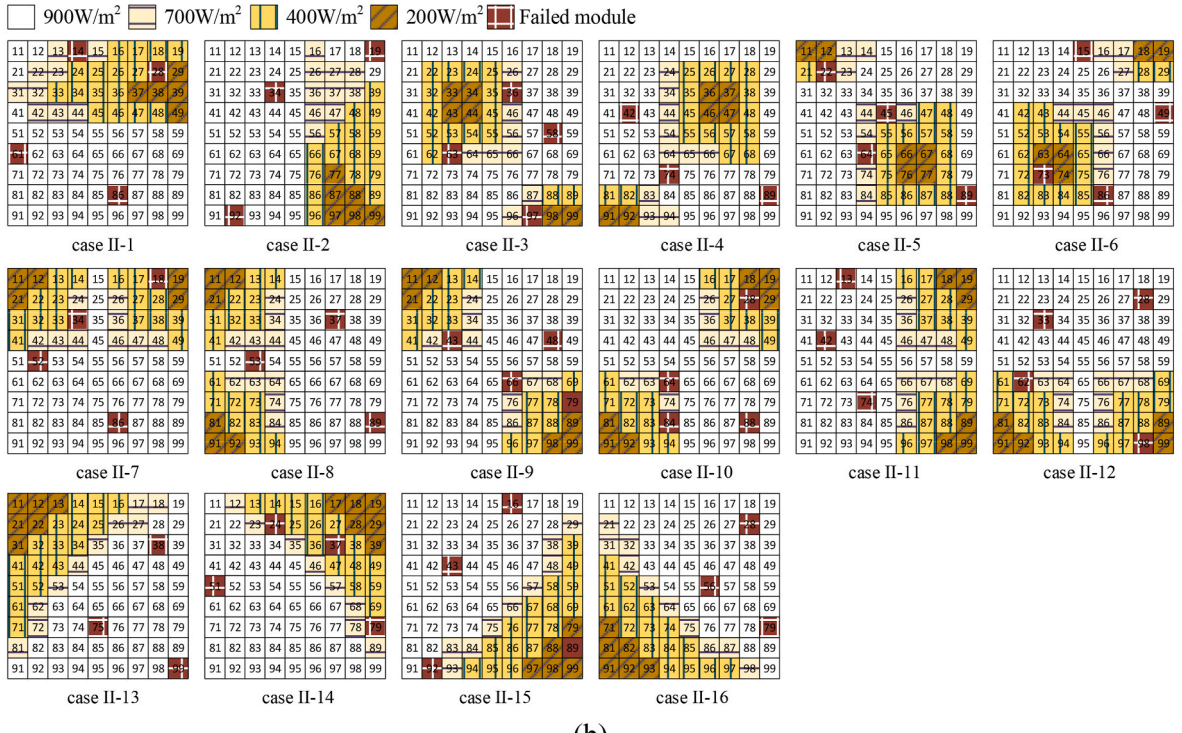

(b)

Fig. 10. Mismatch scenarios: (a) partial shading (Cases I-1 to I-16); and (b) partial shading with random failures (Cases II-1 to II-16).

21	42	63	34	75	16	87	98	59
31	52	73	84	65	96	27	48	19
91	12	83	54	45	26	37	78	69
11	92	53	44	25	66	77	88	39
61	82	33	74	95	56	17	28	49
71	22	43	14	85	36	57	68	99
41	32	23	94	15	76	67	58	89
51	72	93	64	35	86	47	18	29
81	62	13	24	55	46	97	38	79

Fig. 11. Nine-by-nine pattern arrangement with the sudoku method [11].

respectively. The means of the MPP, ML, and ER of the three schemes considered for the sixteen cases are listed in Table 4. From the numerical results of the partial shading pattern, the following conclusions can be drawn.

(1) The proposed MSM reconfiguration solution can improve the power generation in all cases. However, owing to the requirement for the physical repositioning of modules before PV system installation, the sudoku method cannot effectively address the issue of mismatch losses in certain cases, such as Cases I-4, I-5, I-6, I-9, and I-10.

(2) The sudoku method performs better under certain conditions, for example concentrated shadow scenarios; however, the proposed solution can withstand the mismatch condition induced by multiple dispersed shading scenarios. In practice, multiple dispersed shadings often coexist owing to the complex topographies of distributed PV installations. Moreover, the proposed MSM solution outperforms the sudoku method over all the tested scenarios in terms of the mean of the MPP, ML, and ER. The average ML of the MSM solution was 0.255 kW less than that of the sudoku-based arrangement, and the average ER of the proposed MSM solution was 1.250 % higher than that of the sudoku-based arrangement. This is because, in the proposed MSM reconfiguration solution, the PV modules can adjust their positions by controlling the switching matrices. This enabled them to minimize the differences in row irradiances under various mismatch conditions. However, the sudoku method requires the physical

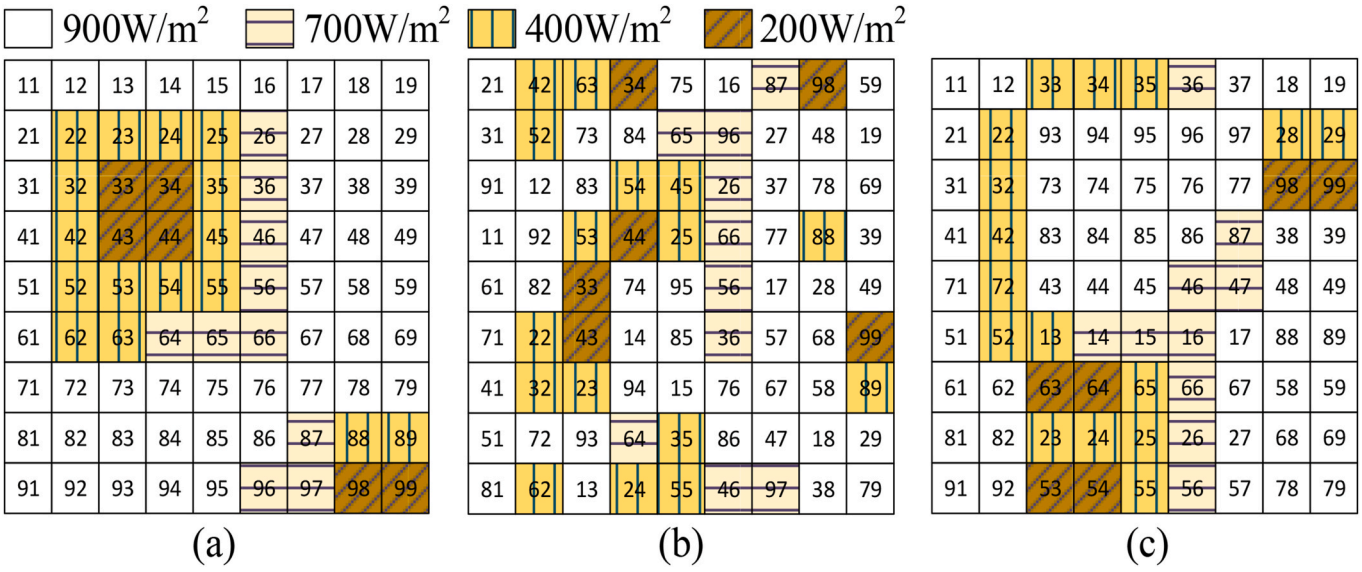

Fig. 12. PV module arrangement for Case I-3: (a) TCT scheme without reconfiguration, (b) reconfiguration using the sudoku method, and (c) reconfiguration using the MSM solution.

Table 2
Position of the MPP of three evaluated schemes for Case I-3.

Original TCT interconnection scheme				Sudoku-based reconfiguration [11]				Proposed reconfiguration solution			
Row	Current	Voltage	MPP	Row	Current	Voltage	MPP	Row	Current	Voltage	MPP
# 3	5.5I_m	9V_m	49.5V_mI_m	# 1	5.5I_m	9V_m	49.5V_mI_m	# 7	6.0I_m	9V_m	54.0V_mI_m
# 4	5.5I_m	–	–	# 4	5.7I_m	8V_m	45.6V_mI_m	# 9	6.0I_m	–	–
# 2	5.9I_m	7V_m	41.3V_mI_m	# 6	6.0I_m	7V_m	42.0V_mI_m	# 3	6.2I_m	7V_m	43.4V_mI_m
# 5	5.9I_m	–	–	# 9	6.2I_m	6V_m	37.2V_mI_m	# 1	6.4I_m	6V_m	38.4V_mI_m
# 9	6.3I_m	5V_m	31.5V_mI_m	# 7	6.6I_m	5V_m	33.0V_mI_m	# 8	6.4I_m	–	–
# 6	6.5I_m	4V_m	26.0V_mI_m	# 3	6.9I_m	4V_m	27.6V_mI_m	# 6	6.5I_m	4V_m	26.0V_mI_m
# 8	6.9I_m	3V_m	20.7V_mI_m	# 2	7.2I_m	3V_m	21.6V_mI_m	# 2	6.6I_m	3V_m	19.8V_mI_m
# 1	8.1I_m	2V_m	16.2V_mI_m	# 5	7.2I_m	–	–	# 5	7.2I_m	2V_m	14.4V_mI_m
# 7	8.1I_m	–	–	# 8	7.4I_m	1V_m	7.4V_mI_m	# 4	7.4I_m	1V_m	7.4V_mI_m

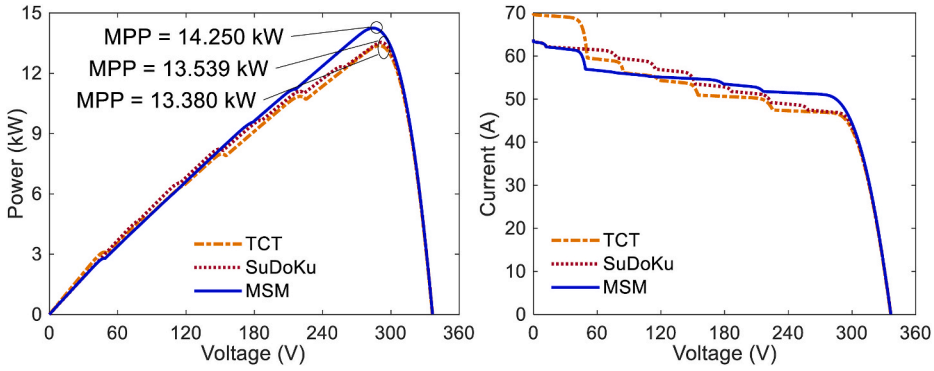

Fig. 13. P–V and I–V characteristics of Case I-3.

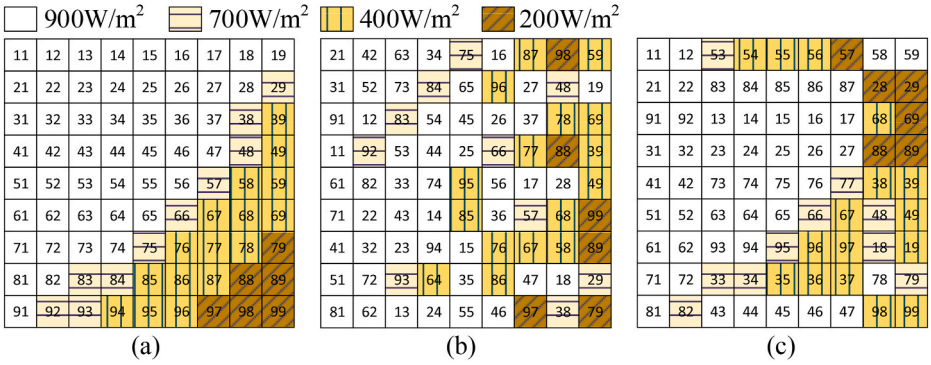

Fig. 14. PV module arrangement for Case I-15: (a) TCT scheme without reconfiguration, (b) reconfiguration using the sudoku method, and (c) reconfiguration using the MSM solution.

Table 3
Position of the MPP of three evaluated schemes for Case I-15.

Original TCT interconnection scheme				Sudoku based arrangement [11]				Proposed reconfiguration solution			
Row	Current	Voltage	MPP	Row	Current	Voltage	MPP	Row	Current	Voltage	MPP
# 9	$4.1I_m$	$9V_m$	$36.9V_mI_m$	# 7	$5.4I_m$	$9V_m$	$48.6V_mI_m$	# 1	$5.7I_m$	$9V_m$	$51.3V_mI_m$
# 8	$4.8I_m$	$8V_m$	$38.4V_mI_m$	# 4	$6.0I_m$	$8V_m$	$48.0V_mI_m$	# 8	$6.0I_m$	$8V_m$	$48.0V_mI_m$
# 7	$5.7I_m$	$7V_m$	$39.9V_mI_m$	# 1	$6.2I_m$	$7V_m$	$43.4V_mI_m$	# 7	$6.2I_m$	$7V_m$	$43.4V_mI_m$
# 6	$6.4I_m$	$6V_m$	$38.4V_mI_m$	# 6	$6.2I_m$	–	–	# 2	$6.7I_m$	$6V_m$	$40.2V_mI_m$
# 5	$6.9I_m$	$5V_m$	$34.5V_mI_m$	# 9	$6.5I_m$	$5V_m$	$32.5V_mI_m$	# 4	$6.7I_m$	–	–
# 3	$7.4I_m$	$4V_m$	$29.6V_mI_m$	# 3	$6.9I_m$	$4V_m$	$27.6V_mI_m$	# 6	$6.7I_m$	–	–
# 4	$7.4I_m$	–	–	# 5	$7.1I_m$	$3V_m$	$21.3V_mI_m$	# 3	$6.9I_m$	$3V_m$	$20.7V_mI_m$
# 2	$7.9I_m$	$2V_m$	$15.8V_mI_m$	# 2	$7.2I_m$	$2V_m$	$14.4V_mI_m$	# 5	$6.9I_m$	–	–
# 1	$8.1I_m$	$1V_m$	$8.1V_mI_m$	# 8	$7.2I_m$	–	–	# 9	$6.9I_m$	–	–

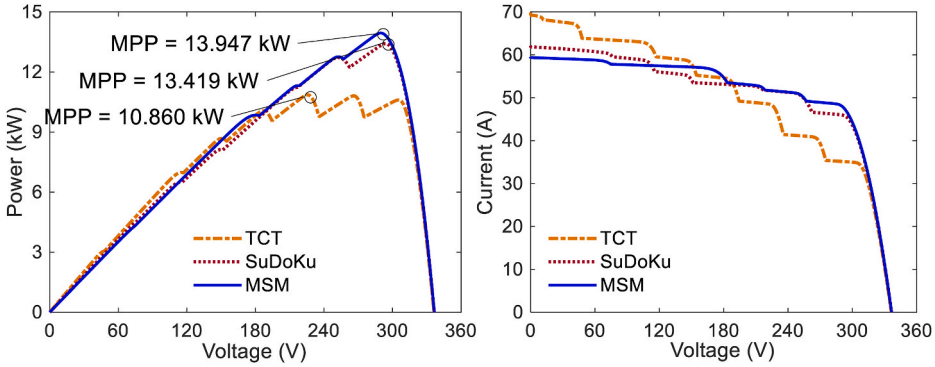

Fig. 15. P–V and I–V characteristics of Case I-15.

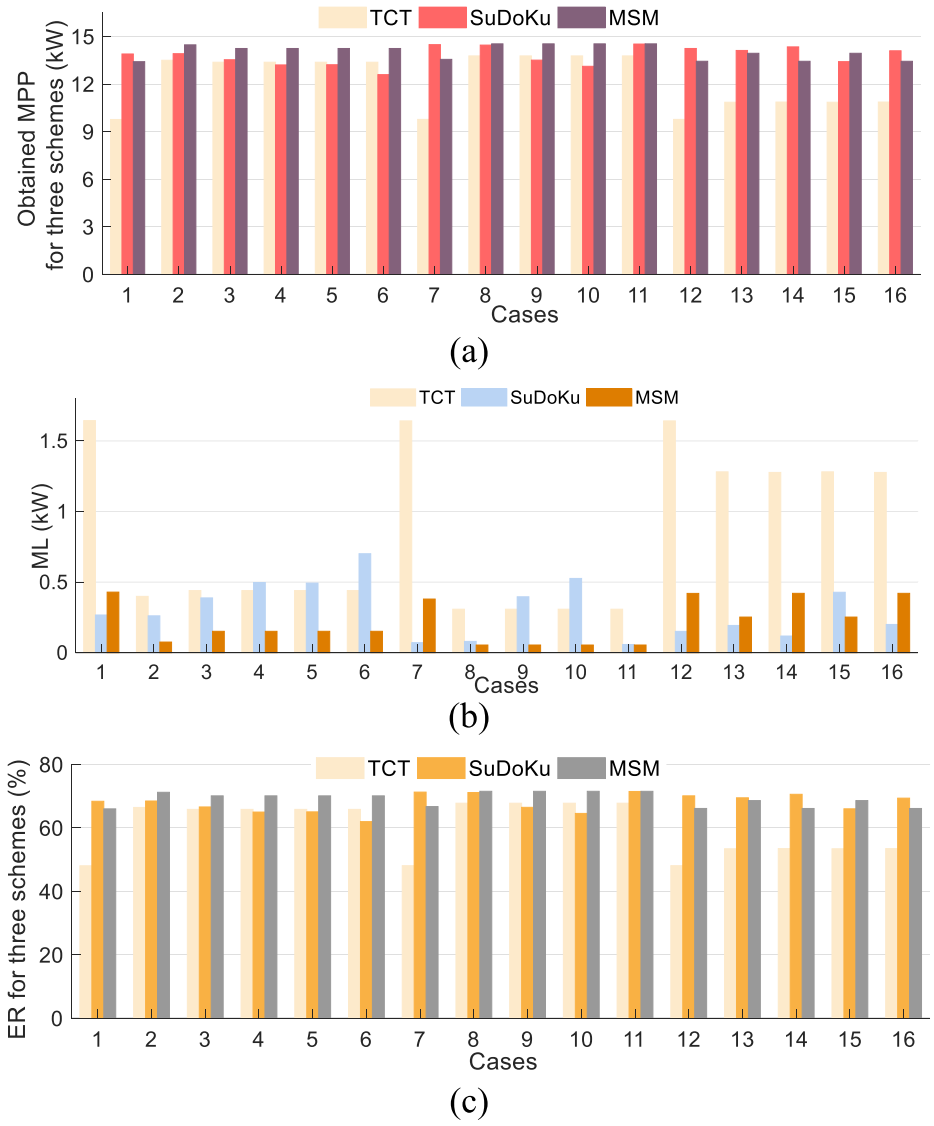

Fig. 16. Performance comparison of different schemes for all test cases (Cases I-1 to I-16): (a) MPP; (b) ML; and (c) ER.

Table 4
Mean of the MPP, ML, and ER of three considered schemes for Cases I-1 to I-16.

	MPP (kW)	ML (kW)	ER (%)
TCT	12.183	2.520	59.963
Sudoku	13.797	0.906	67.906
MSM	14.052	0.651	69.156

repositioning of modules before the installation of the PV system. Consequently, the MSM method can effectively address all types of mismatch conditions.

Furthermore, the calculated standard deviation of the MPP of the MSM solution was 0.123 kW, which is less than that of the sudoku-based arrangement. Furthermore, according to Fig. 17 (a) and (b), the degree of dispersion of the MPPs of the sudoku-based arrangement is larger than that of the proposed MSM solution.

5.2. *Partial shading with random failures pattern*

4) Test case 3: two partial shadows with random failures (Case II-3)

The shaded and failed module positions in the mismatch scenario of Case II-3 are shown in Fig. 18(a). The sudoku method and MSM solution were applied, and the arrangements are illustrated in Fig. 18(b) and (c), respectively. The number of switch actions in the MSM solution for Case II-3 was 26.

For the three considered schemes, the calculated voltage and current values and obtained MPPs of the PV array are presented in Table 5. It is observed that the highest MPP 48.0 V_mI_m is produced by the proposed reconfiguration solution as compared to TCT (43.2 V_mI_m) and sudoku (45.9 V_mI_m) methods.

The P–V characteristics and I–V characteristics of Case II-3 are shown in Fig. 19. From the figures, the MPP obtained for the proposed MSM reconfiguration solution is 13.089 kW, which is significantly improved compared with the TCT interconnection scheme (11.979 kW) and the sudoku-based arrangement (12.573 kW).

5) Test case 4: a corner shadow with random failures (Case II-15)

The shaded and failed module positions in the mismatch scenario of CaseII-15 are shown in Fig. 20(a). The arrangements realized by the sudoku method and MSM solution are shown in Fig. 20 (b) and (c), respectively. The number of switch actions in the MSM solution for Case

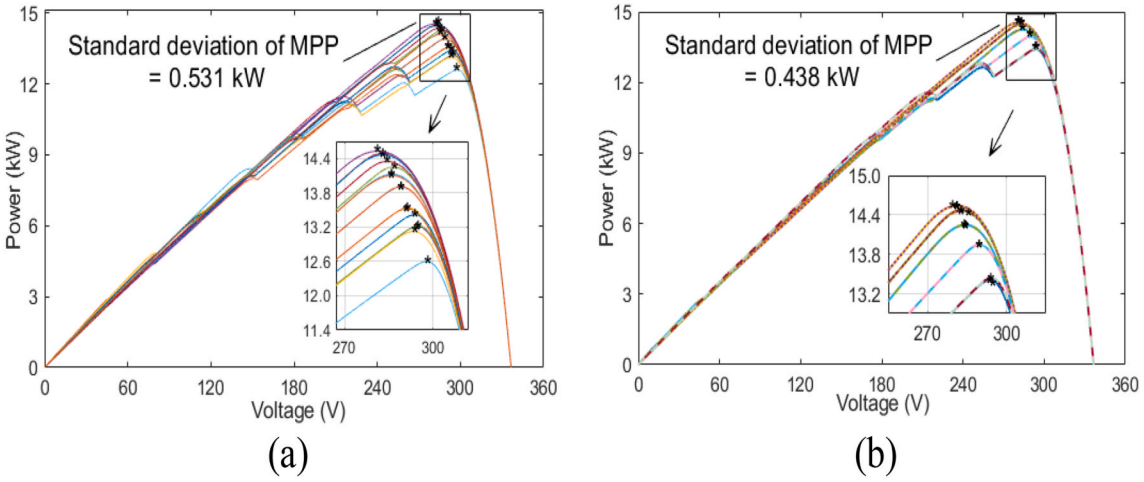

Fig. 17. P–V characteristics of Cases I-1 to I-16: (a) sudoku based arrangement; and (b) the proposed reconfiguration solution.

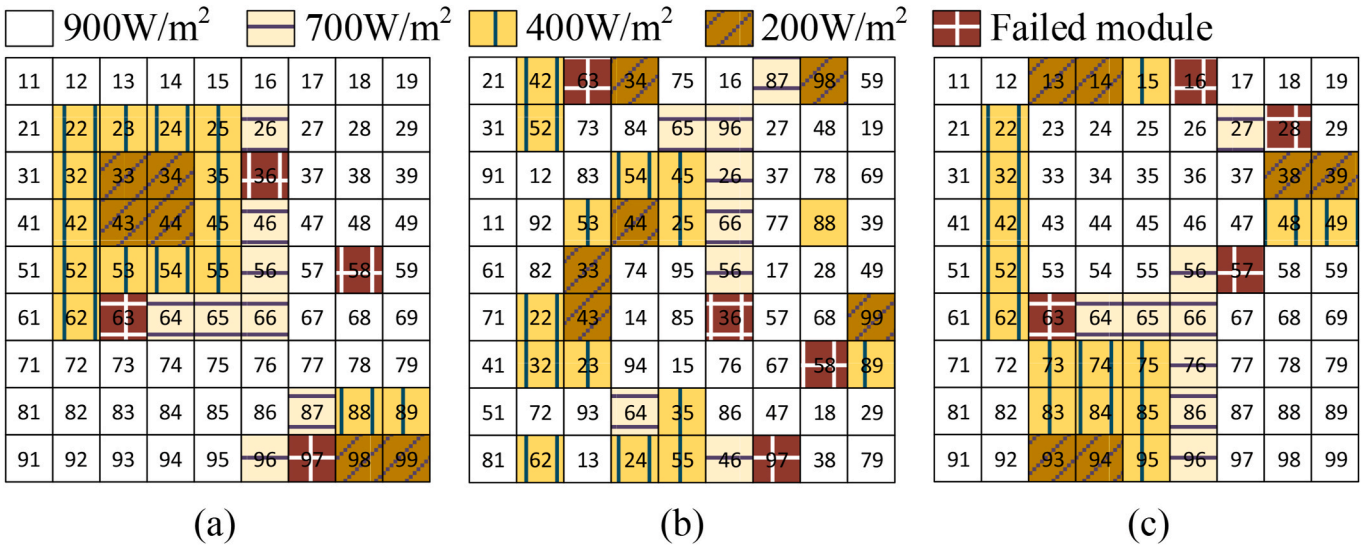

Fig. 18. PV module arrangement for Case II-3: (a) TCT scheme without reconfiguration; (b) reconfiguration using sudoku method; and (c) reconfiguration using MSM solution.

Table 5
Position of the MPP of the three evaluated schemes for Case II-3.

original TCT interconnection scheme				Sudoku-based arrangement [11]				Proposed reconfiguration solution			
Row	Current	Voltage	MPP	Row	Current	Voltage	MPP	Row	Current	Voltage	MPP
# 3	$4.8I_m$	$\underline{9V_m}$	$\underline{43.2V_mI_m}$	# 1	$5.1I_m$	$\underline{9V_m}$	$\underline{45.9V_mI_m}$	# 1	$5.3I_m$	$9V_m$	$47.7V_mI_m$
# 5	$5.0I_m$	$8V_m$	$40.0V_mI_m$	# 6	$5.3I_m$	$8V_m$	$42.4V_mI_m$	# 9	$6.0I_m$	$\underline{8V_m}$	$\underline{48.0V_mI_m}$
# 4	$5.5I_m$	$7V_m$	$38.5V_mI_m$	# 9	$5.5I_m$	$7V_m$	$38.5V_mI_m$	# 6	$6.1I_m$	$7V_m$	$42.7V_mI_m$
# 9	$5.6I_m$	$6V_m$	$33.6V_mI_m$	# 4	$5.7I_m$	$6V_m$	$34.2V_mI_m$	# 3	$6.2I_m$	$6V_m$	$37.2V_mI_m$
# 2	$5.9I_m$	$5V_m$	$29.5V_mI_m$	# 7	$5.7I_m$	–	–	# 7	$6.4I_m$	$5V_m$	$32.0V_mI_m$
# 6	$6.1I_m$	$4V_m$	$24.4V_mI_m$	# 3	$6.9I_m$	$4V_m$	$27.6V_mI_m$	# 8	$6.4I_m$	–	–
# 8	$6.9I_m$	$3V_m$	$20.7V_mI_m$	# 2	$7.2I_m$	$3V_m$	$21.6V_mI_m$	# 2	$6.5I_m$	$4V_m$	$19.5V_mI_m$
# 1	$8.1I_m$	$2V_m$	$16.2V_mI_m$	# 5	$7.2I_m$	–	–	# 5	$6.5I_m$	–	–
# 7	$8.1I_m$	–	–	# 8	$7.4I_m$	$1V_m$	$7.4V_mI_m$	# 4	$6.6I_m$	$1V_m$	$6.6V_mI_m$

II-15 was 20.

The calculated row current and voltage values and obtained MPPs of the PV array for Case II-15 are presented in Table 6. The highest MPP (51.3 V_mI_m) is produced by the proposed reconfiguration solution, compared to the TCT (39.9 V_mI_m) and sudoku (46.8 V_mI_m) methods.

The P–V and I–V characteristics of Case II-15 are shown in Fig. 21. From the figure, the MPP obtained for the proposed MSM solution is 13.704 kW, which is significantly improved compared with the TCT interconnection scheme (10.764 kW) and the sudoku-based arrangement (12.630 kW).

6) Statistics of all test cases (Case II-1 to II-16)

The MPP, ML, and ER values of the various configurations for Cases II-1 to II-16 are shown in Fig. 22 (a), (b), and (c), respectively. The means of the MPP, ML, and ER of the three schemes considered for the

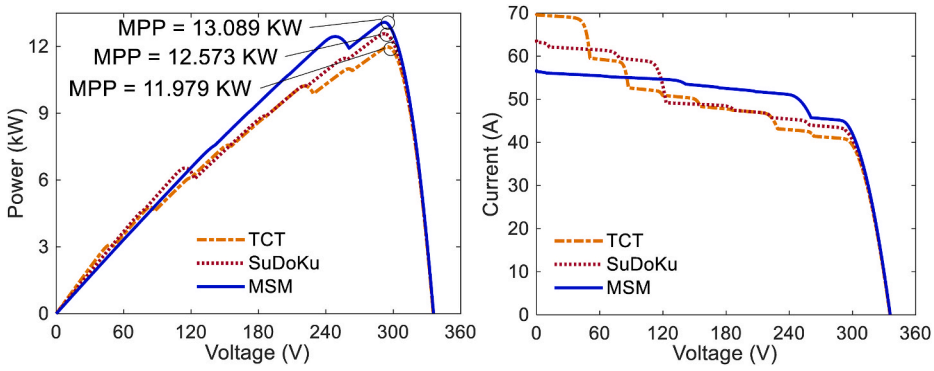

Fig. 19. P–V and I–V characteristics of Case II-3.

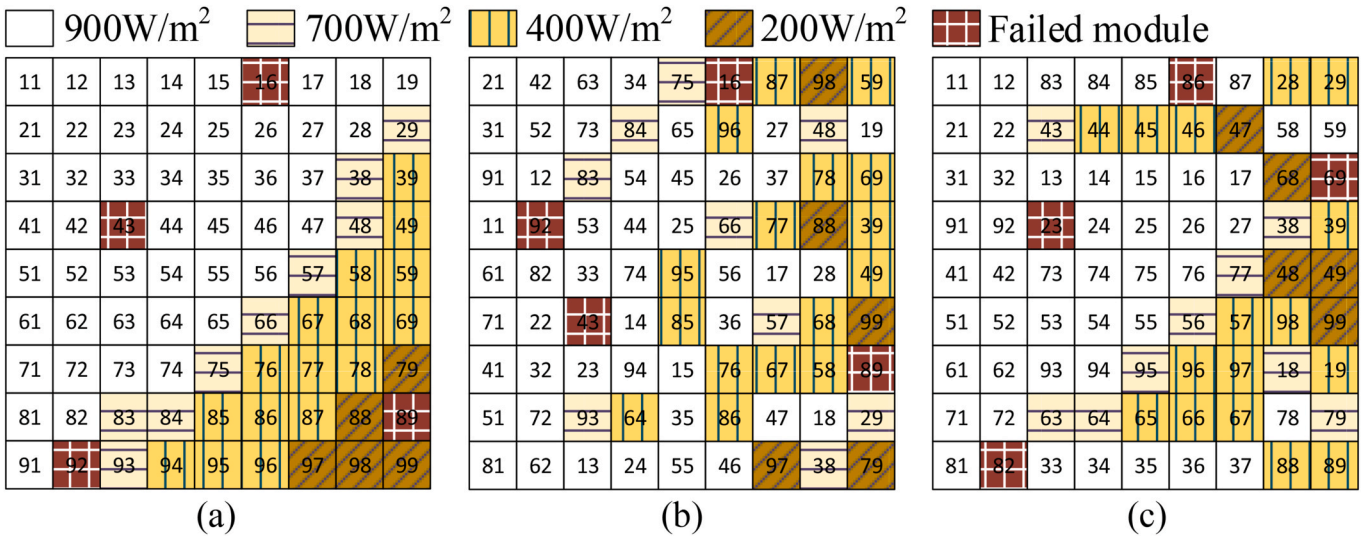

Fig. 20. PV module arrangement for Case II-15: (a) TCT scheme without reconfiguration, (b) reconfiguration using the sudoku method, and (c) reconfiguration using the MSM solution.

Table 6
Position of the MPP of three evaluated schemes for Case II-15.

original TCT interconnection scheme				SuDoKu based arrangement [11]				Proposed reconfiguration solution			
Row	Current	Voltage	MPP	Row	Current	Voltage	MPP	Row	Current	Voltage	MPP
# 9	$3.4I_m$	$9V_m$	$30.6V_mI_m$	# 7	$5.2I_m$	$\underline{9V_m}$	$\underline{46.8V_mI_m}$	# 2	$\underline{5.7I_m}$	$\underline{9V_m}$	$\underline{51.3V_mI_m}$
# 8	$4.6I_m$	$8V_m$	$36.8V_mI_m$	# 1	$5.3I_m$	$8V_m$	$42.4V_mI_m$	# 8	$6.0I_m$	$8V_m$	$48.0V_mI_m$
# 7	$5.7I_m$	$\underline{7V_m}$	$\underline{39.9V_mI_m}$	# 4	$5.3I_m$	–	–	# 1	$6.2I_m$	$7V_m$	$43.4V_mI_m$
# 6	$6.4I_m$	$6V_m$	$38.4V_mI_m$	# 6	$5.3I_m$	–	–	# 6	$6.2I_m$	–	–
# 4	$6.5I_m$	$5V_m$	$32.5V_mI_m$	# 9	$6.5I_m$	$5V_m$	$32.5V_mI_m$	# 7	$6.2I_m$	–	–
# 5	$6.9I_m$	$4V_m$	$27.6V_mI_m$	# 3	$6.9I_m$	$4V_m$	$27.6V_mI_m$	# 9	$6.2I_m$	–	–
# 1	$7.2I_m$	$3V_m$	$21.6V_mI_m$	# 5	$7.1I_m$	$3V_m$	$21.3V_mI_m$	# 3	$6.5I_m$	$3V_m$	$19.5V_mI_m$
# 3	$7.4I_m$	$2V_m$	$14.8V_mI_m$	# 2	$7.2I_m$	$2V_m$	$14.4V_mI_m$	# 4	$6.5I_m$	–	–
# 2	$7.9I_m$	$1V_m$	$7.9V_mI_m$	# 8	$7.2I_m$	–	–	# 5	$6.5I_m$	–	–

sixteen cases are listed in Table 7. The bar charts and table show that the performance of the proposed MSM reconfiguration solution is better than that of the sudoku method in all cases. The average mismatch loss of the MSM solution was 1.293 kW lower than that of the sudoku method, and the average execution ratio of the proposed reconfiguration solution was 6.364 % higher than that of the sudoku-based arrangement.

The standard deviation of the MPP of the proposed MSM reconfiguration solution was 0.237 kW, which was less than that of the sudoku-based arrangement. Furthermore, the results in Fig. 23 (a) and (b) show that the dispersion degree of the MPPs of the sudoku-based arrangement is larger than that of the proposed MSM solution.

5.3. Testbed validation

Fig. 24 shows the testbed containing 2 × 11 PV modules with a 280 W output rating and I–V curve testers that can collect IV curves for each PV module. To simulate the mismatch condition, the PV panels are shaded by a shade cloth, and some typical I–V curves are shown in Fig. 24. It can be found that the I–V curve of 100 % shading in a cell row is close to partial shading in a module. This is because the cells in a PV module are connected in series and the output drop of one cell affects the entire PV module. After obtaining the I–V curves of each PV module and combining the size of the PV array and the location of the switching matrices, the optimal switching operation scheme can be obtained

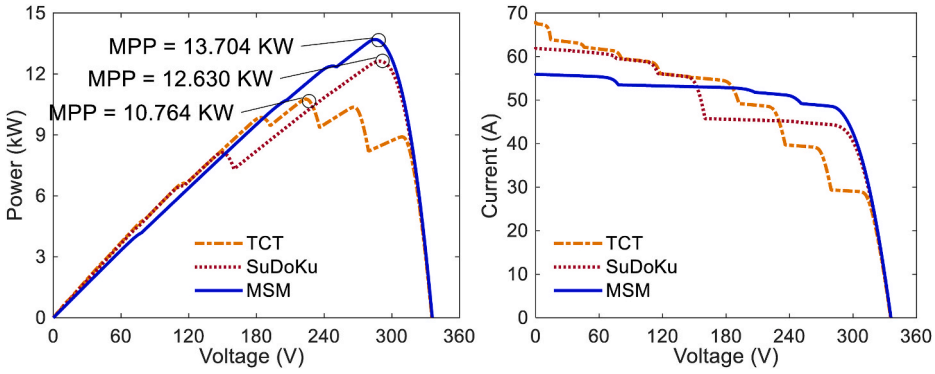

Fig. 21. P–V and I–V characteristics of Case II-15.

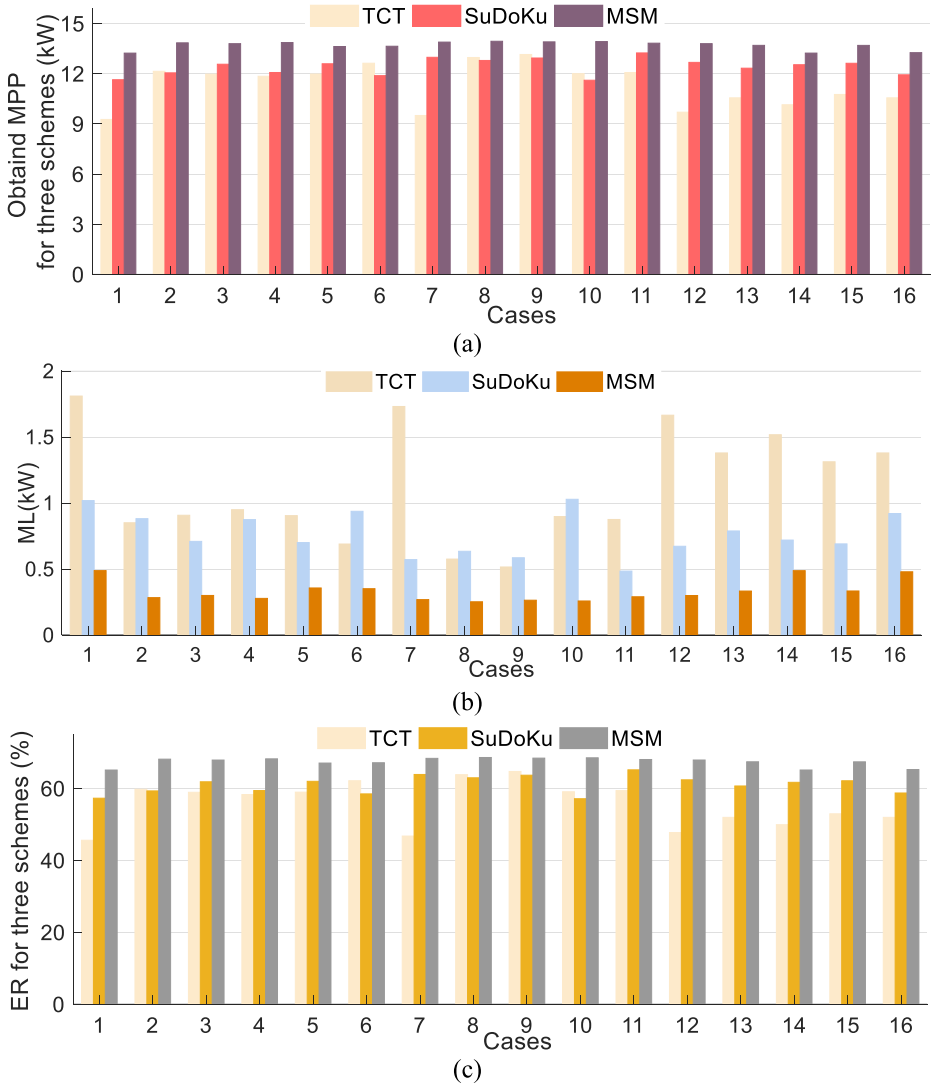

Fig. 22. Performance comparison of different schemes for all test cases (Cases II-1 to II-16): (a) MPP, (b) ML, and (c) ER.

Table 7
Mean of the MPP, ML, and ER of three schemes for Cases II-1 to II-16.

	MPP (kW)	ML (kW)	ER (%)
TCT	11.334	3.369	55.779
Sudoku	12.411	2.292	61.079
MSM	13.704	0.999	67.443

through the optimization reconfiguration algorithm (proposed in Section III).

PV modules with four different shading levels were considered to simulate PV array mismatch conditions, as shown in Fig. 25(a). The switching statutes and PV output curves before and after the reconfiguration are shown in Fig. 25(b) and (c), respectively. The closed switches are indicated by red circles. From the figures, the MPP obtained

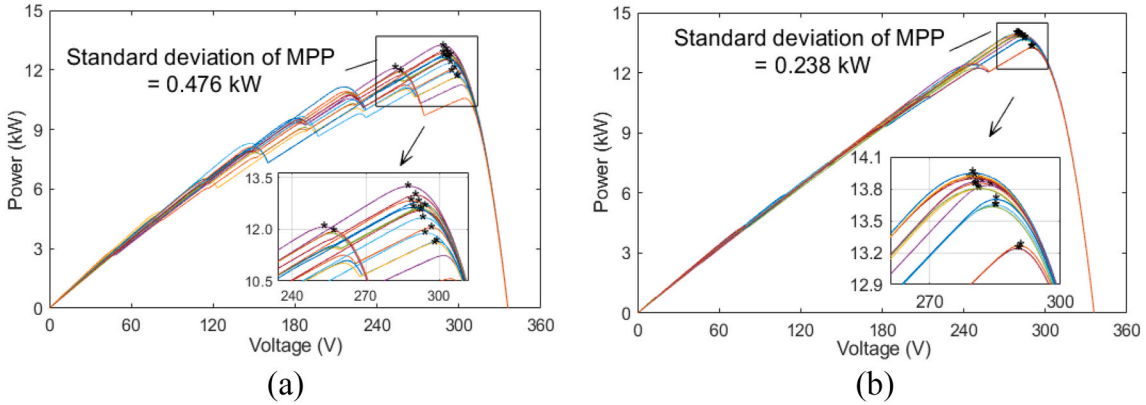

Fig. 23. P–V characteristics of Cases II-1 to II-16: (a) sudoku-based arrangement and (b) the proposed MSM reconfiguration solution.

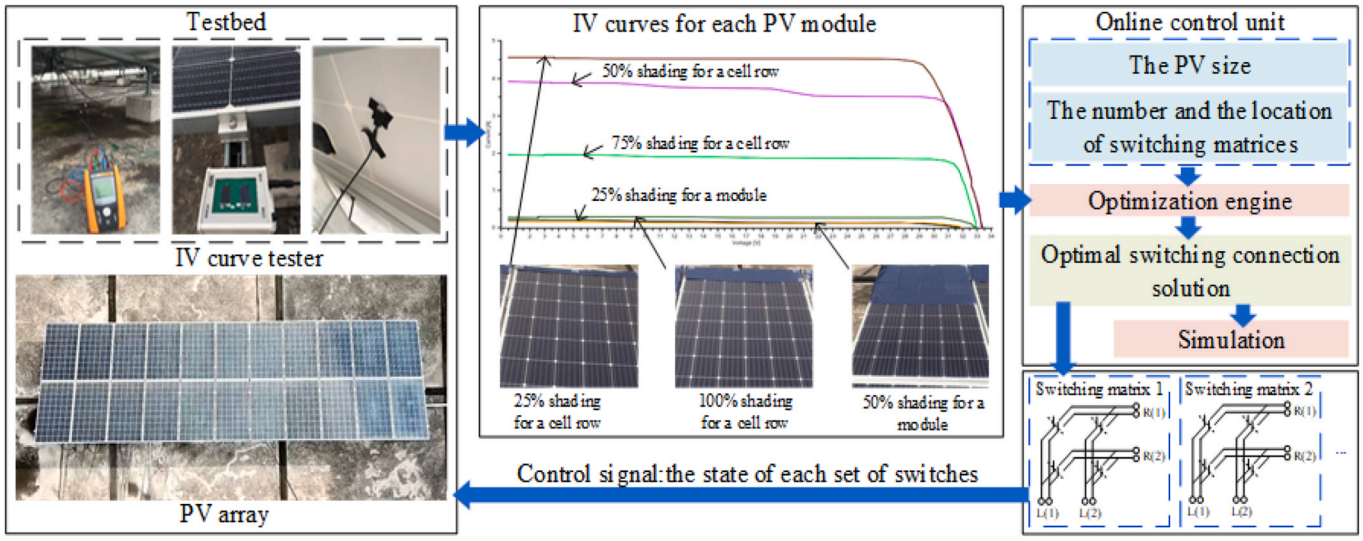

Fig. 24. Testbed validation of a dynamic topology reconfiguration solution.

for the proposed reconfiguration solution is 3.396 kW, which is an 11.31 % increase, compared to the PV array without reconfiguration (3.012 kW).

5.4. Cost-benefit analysis

This section presents a cost–benefit analysis that considers the total installation cost of the proposed reconfiguration method and the profit from power generation improvement by adopting the proposed method.

Mismatch loss problems occur in distributed PV systems because of the shading caused by surrounding buildings, dust, bird droppings, fallen leaves, module defects, and even failures. Thus, the factors leading to mismatch losses are mostly random, and the degree of mismatch loss varies depending on the operational environment. Therefore, the increase obtained using the dynamic reconfiguration method was difficult to estimate. Therefore, a mismatch condition of five working hours and an average power reduction of 35 % are considered in this study, and a power generation improvement of 10 % for the PV array can be achieved for simplicity, as suggested in Ref. [30].

The hardware of the proposed dynamic PV reconfiguration method includes a PV monitoring instrument, switching matrix, and driving circuit [30]. The selected measuring instruments, that is, the voltage and current sensors, are useful for PV panels with voltage margins between 0 and 25 V and current margins between 0 and 20 A [31]. In the switching matrix, each switch consists of a set of electromechanical relays and a semiconductor device (e.g., a MOSFET). One MOSFET must be connected to a set of relays and one driver must drive one MOSFET [30]. The prices of the components are listed in Table 8.

The number of required components that should be used in the 9 × 9 and 9 × 20 TC T-interconnected PV arrays with two switching matrices are shown in Table 9, as well as the total installation cost. As mentioned previously, the size of the switching matrix is determined only by the number of PV rows. Therefore, for the 9 × 20 PV array, the number of relays, MOSFETs, and required drivers did not increase.

For the 9 × 9 and 9 × 20 TC T-interconnected PV array with 250 W module capacity, considering that the lifetime of the PV array is twenty-five years and the sale price is $83 per megawatt-hour [32], the economic estimations of the proposed reconfiguration method are shown in Table 10. This indicates that a PV array with sizes of 9 × 9 and 9 × 20 can profit in approximately ten and five years, respectively.

6. Conclusion

This study presented the performance of a PV-array reconfiguration solution, namely MSM, for a TCT-interconnected PV array under mismatch conditions. In this method, the current and voltage values of each module were collected using electric measurement sensors and sent to the control unit to compute and determine the optimal electrical connection of the PV array. In addition, the hardware-switching matrix structure and reconfiguration algorithm designed in the MSM solution

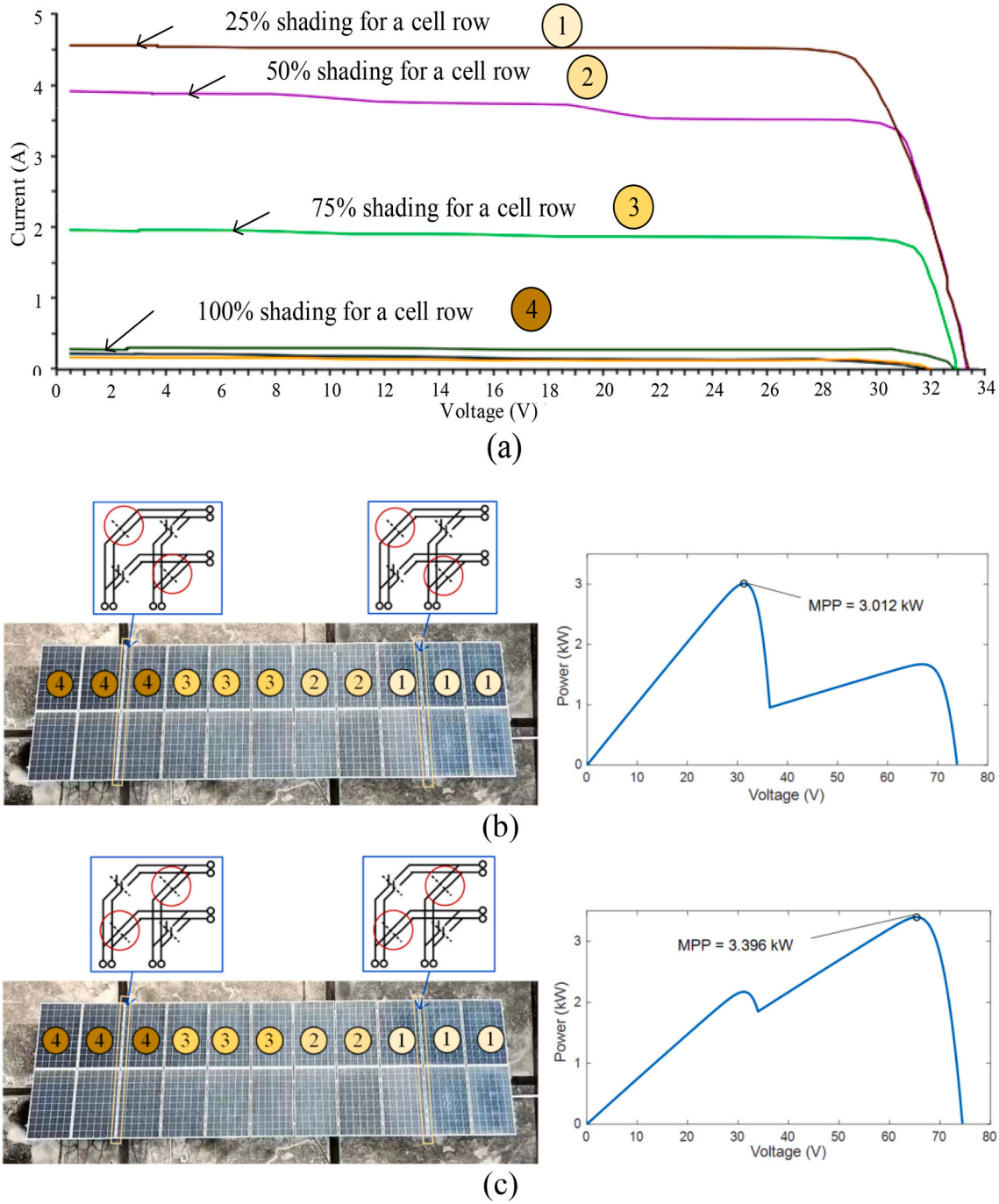

Fig. 25. Results of the reconfiguration experiment. (a) IV curves for four different shading modules, switching statues, and PV output curves for (b) before reconfiguration and (c) after reconfiguration.

Table 8
Price of the required hardware of the dynamic PV reconfiguration method.

Component	Brand	Price ($)
Voltage sensor	MF301	0.38
Current sensor	ACS712	1.30
Relay	Hongfa Europe GMbH	2.95
MOSFET	IPB08CN10 N	1.44
Driver	MAX845	3.63

are available for any PV array size. The proposed reconfiguration solution was extensively assessed under mismatched conditions for a range of partial shading patterns and partial shading with random failure

Table 9
Number of components and total cost of the proposed MSM reconfiguration solution applied to 9 × 9 and 9 × 20 TC T topology.

	9 × 9 TC T-based PV array	9 × 20 TC T-based PV array
The number of voltage sensor	81	180
The number of current sensor	81	180
The number of relay	324	324
The number of MOSFET	162	162
The number of driver	162	162
Total cost ($)	1913.2	2079.5

Table 10
Economic estimates of the proposed MSM reconfiguration solution applied to 9 × 9 and 9 × 20 TC T topologies.

Period (*n* years)	Profit ($)	
	9 × 9 TC T-based PV array	9 × 20 TC T-based PV array
n = 5	−916.3	135.8
n = 10	80.6	2351.1
n = 15	1077.5	4566.5
n = 20	2074.4	6781.8
n = 25	3071.3	8997.1

patterns. Simulations showed better reconfiguration results using the proposed method compared with the existing sudoku-based arrangement and the original TCT interconnection scheme. The proposed reconfiguration solution was evaluated by analyzing the P–V and I–V curves. Moreover, three main parameters and standard deviations of the MPP for each pattern were considered. The proposed MSM reconfiguration solution always mitigated mismatch losses, and the sudoku-based physical relocation reconfiguration were not sufficiently flexible to withstand the impact of mismatch conditions, for example, multiple partial shadows and random module failures, on the power generation of the PV array. The numerical results confirmed the feasibility, effectiveness, and flexibility of the proposed reconfiguration solution for promoting PV power generation, thereby enhancing the utilization of renewable energy sources. Furthermore, a cost-benefit analysis was presented to demonstrate the economic feasibility of the work in engineering deployment.

In the proposed MSM reconfiguration solution, the design of the number of switching matrices is a tradeoff between cost and flexibility. For future work, the number and location of switches need to be further investigated for different scenarios of PV plants to further enhance the efficiency of the proposed solution. In addition, the effectiveness and cost-benefit of the proposed MSM reconfiguration method need to be further explored and validated in large-scale PV power-generation systems.

CRediT authorship contribution statement

Xiaolun Fang: Conceptualization, Methodology, Data curation, Writing - review & editing, Writing - original draft. **Qiang Yang:** Supervision, Writing - review & editing.

Declaration of competing interest

The authors declare that they have no known competing financial interests or personal relationships that could have appeared to influence the work reported in this paper.

Data availability

No data was used for the research described in the article.

Acknowledgments

This work is supported by the “Pioneer” and “Leading Goose” R&D Program of Zhejiang (2022C01239), the Special Support Plan for Zhejiang Province High-level Talents (2022R52012) and the National Natural Science Foundation of China (52177119).

References

[1] Krishna GS, Moger T. A novel adaptive dynamic photovoltaic reconfiguration system to mitigate mismatch effects. Renew Sustain Energy Rev 2021;141.
[2] Solar power statistics in China 2021. 2022 [Online], https://www.solarfeeds.com/mag/solar-power-statistics-in-china-2021/.
[3] El-Dein MZS, Kazerani M, Salama MMA. An optimal total cross tied interconnection for reducing mismatch losses in photovoltaic arrays. IEEE Trans Sustain Energy Jan. 2013;4:99–107.
[4] Liu L, Meng X, Liu C. A review of maximum power point tracking methods of PV power system at uniform and partial shading. Renew Sustain Energy Rev 2016;53:1500–7.
[5] Lappalainen K, Velkealahti S. Photovoltaic mismatch losses caused by moving clouds. Sol Energy 2017;158:455–61.
[6] Balato M, Costanzo L, Vitelli M. Series–Parallel PV array re-configuration: maximization of the extraction of energy and much more. Appl Energy Dec.2015;159(1):145–60.
[7] Omairi A, Ismail ZH, Danapalasingam KA, et al. Power harvesting in wireless sensor networks and its adaptation with maximum power point tracking: current technology and future directions. IEEE Internet Things J Dec. 2017;4(6):2104–15.
[8] Pillaib DS, Rama JP, Nihanthb MSS, et al. A simple, sensorless and fixed reconfiguration scheme for maximum power enhancement in PV systems. Energy Convers Manag 2018;172:402–17. Step.
[9] Krishna GS, Moger T. Reconfiguration strategies for reducing partial shading effects in photovoltaic arrays: state of the art. Sol Energy Apr.2019;182:429–52.
[10] Rani BI, Ilango GS, Nagamani C. Enhanced power generation from PV array under partial shading conditions by shade dispersion using su do ku configuration. IEEE Trans Sustain Energy Jul. 2013;4(3):594–601.
[11] Krishna GS, Moger T. Improved SuDoKu reconfguration technique for total-cross-tied PV array to enhance maximum power under partial shading conditions. Renew Sustain Energy Rev Jul. 2019;109:333–48.
[12] Sahu HS, Nayak SK, Mishra S. Maximizing the power generation of a partially shaded PV array. IEEE Journal of Emerging and Selected Topics in Power Electronics Jun. 2016;4(2):626–37.
[13] Yadav AS, Pachauri RK, Chauhan YK, et al. Performance enhancement of partially shaded PV array using novel shade dispersion effect on magic-square puzzle configuration. Sol Energy Mar.2019;144:780–97.
[14] Dhanalakshmi B, Rajasekar N. Dominance square based array reconfiguration scheme for power loss reduction in solar PhotoVoltaic (PV) systems, vol. 156. Energy Conversion and Management; Jan.2018. p. 84–102.
[15] Dhanalakshmi B, Rajasekar N. A novel Competence Square based PV array reconfiguration technique for solar PV maximum power extraction. Energy Convers Manag Oct.2018;174:897–912.
[16] Belhaouas N, Cheikh MSA, Agathoklis P, et al. PV array power output maximization under partial shading using new shifted PV array arrangements. Appl Energy Feb.2017;187:326–37.
[17] Hu Y, Zhang J, Li P, et al. Non-uniform aged modules reconfiguration for large-scale PV array. IEEE Trans Device Mater Reliab 2017;17:560–9. Step.
[18] Babu TS, Ram JP, Dragičević T, et al. Particle swarm optimization based solar PV array reconfiguration of the maximum power extraction under partial shading conditions. IEEE Trans Sustain Energy Jan.2018;9(1):74–85.
[19] Deshkar SN, Dhale SB, Mukherjee JS, et al. Solar PV array reconfiguration under partial shading conditions for maximum power extraction using genetic algorithm. Renew Sustain Energy Rev Mar.2015;43:102–10.
[20] Alalmad M, Chaaban MA, Lau S, et al. An adaptive utility interactive photovoltaic system based on a flexible switch matrix to optimize performance in real-time. Sol Energy Mar.2012;86:951–63.
[21] Karakose M, Baygin M, Parlak KS. A new real-time reconfiguration approach based on neural network in partial shading for PV arrays. In: 2014 international conference on renewable energy research and application. Milwaukee, WI: ICRERA); 2014. p. 633–7.
[22] Karakose M, Baygin M, Baygin N, et al. An intelligent reconfiguration approach based on fuzzy partitioning in PV arrays. In: 2014 IEEE international symposium on innovations in intelligent systems and applications. Proceedings, Alberobello; 2014. p. 356–60.
[23] Rao PS, Ilango GS, Nagamani C. Maximum power from PV arrays using a fixed configuration under different shading conditions. IEEE J Photovoltaics 2014;4(2):679–86.
[24] Rhaman MM, Matin MA. Organic solar cells: historical developments and challenges. In: 2015 international conference on advances in electrical engineering. ICAEE); 2015. p. 26–9.
[25] Thayalan DT, Lee H, Park J. Low-cost high-efficiency discrete current sensing method using bypass switch for PV systems. IEEE Trans Instrum Meas 2014;63(4):769–80.
[26] Lofberg J. ALMIP: a toolbox for modeling and optimization in MATLAB,” *2004 IEEE International Conference on Robotics and Automation*. 2004. p. 284–9. New Orleans, LA.
[27] GUROBI OPTIMIZATION Solve Complex Problems Fast. [Online]. Available: https://www.gurobi.com/.
[28] Velasco-Quesada G, Guinjoan-Gispert F, Pique-Lopez R, et al. Electrical PV array reconfiguration strategy for energy extraction improvement in grid-connected PV systems. IEEE Trans Ind Electron 2009;56(11):4319–31.
[29] Zhao Q, Wang G, Liang D, et al. Research on multi-objective optimization of integrated energy system considering integrated demand response. In: 2021 IEEE/IAS industrial and commercial power system asia. I&CPS Asia); 2021. p. 1572–8.
[30] Schettino G, Pellitteri F, Ala G, et al. Dynamic reconfiguration systems for PV plant: technical and economic analysis. Energies 2020;13:1–21.
[31] Hall current sensor module ACS712 module. Available online: https://www.aliexpress.com.
[32] Solar PV generators receive higher electricity prices than other technologies – eia. Available online: https://renewablesnow.com/news/solar-pv-generators-receive-higher-electricity-prices-than-other-technologies-eia-716914/.